Treatment of the solar radiation by spatial and temporal discretization for modeling the thermal response of arch dams.

D. Santillán[1], E. Salete[2], D.J. Vicente[3] and M.Á. Toledo[4]

ABSTRACT.

A methodology for computing thermal loads in arch dams is proposed. The methodology considers the non-uniform distribution of solar insolation over dam faces due to shading, curvature of dam faces, orientation and slopes. Since in most cases mean daily global solar radiation is that only available, a methodology for estimating hourly solar energy reaching dam faces is described. The methodology is applied to a case study where observations from 21 thermometers embedded in the concrete and where data of climatic variables are available. The concrete temperature field is successfully computed, with good agreement between observations and predictions. The proposed methodology is compared with other approaches and the consequences on the stress calculations are analyzed.

Key words: Thermal analysis, Arch dam, Finite element method, Solar radiation, Dam safety

[1] Lecturer, Technical University of Madrid. Department of Civil Engineering: Hydraulic and Energy Engineering, C/Profesor Aranguren s/n, 28040 Madrid, Spain (corresponding author). E-mail: david.santillan@upm.es.

[2] Professor, Technical University of Madrid. Department of Civil Engineering: Hydraulic and Energy Engineering, C/Profesor Aranguren s/n, 28040 Madrid, Spain.

[3] Ph.D. Candidate. Technical University of Madrid. Department of Civil Engineering: Hydraulic and Energy Engineering, C/Profesor Aranguren s/n, 28040 Madrid, Spain.

[4] Professor, Technical University of Madrid. Department of Civil Engineering: Hydraulic and Energy Engineering, C/Profesor Aranguren s/n, 28040 Madrid, Spain.

Doi: https://doi.org/10.1061/(ASCE)EM.1943-7889.0000801

INTRODUCTION.

Thermal loads are defined as temperature changes which cause stress in a structure. These loads are important in arch dams where changes in the temperature field from the distribution in the contraction joint grouting day will cause stress. The purpose of the grouting operation is to bind the construction blocks together in order that the dam works as a monolithic structure (US Department of the Interior, 1977). Temperature changes during service life may affect the integrity of the structure due to excessive stress which could lead to cracking. In addition, the second most major repairs in dams during operation are caused by external temperature variations (Douglas 2002). Furthermore, thermal loads are of special interest in monitoring existing structures.

Concrete temperature mainly varies due to the heat flow between the dam surface and the surrounding environment. Inside the dam, heat transfer occurs due to the physical mechanism of conduction, governed by the heat diffusion equation (Incropera *et al*. 2011). The dam exchanges heat with the surrounding environment thanks to the convection, the radiation and the evaporative cooling.

The convection is the heat exchange caused by temperature difference between the bulk of air and the air neighboring the surface of the structure. Radiation heat transfer is made through long wave radiation and short wave radiation. Long wave radiation is related to energy emission of a body because of its temperature. An energy balance of the dam is found by calculating the difference between the long wave radiation that is being emitted by the concrete and the incident energy being absorbed by the dam. That energy is emitted by the surrounding environment -neighboring objects, sky, clouds...- and depends on the temperature of the environment. However, the temperature of the

41 sky during night time is often lower than the environmental one. This result in a night
42 cooling and the phenomena is considered by using an apparent night sky temperature
43 when energy fluxes due to long wave radiation exchange are computed (Azenha 2009).
44 The short wave radiation is considered for energy emitted by the sun. The evaporative
45 cooling is a mechanism of heat loss due to water evaporation.

46 The temporal and spatial distributions of irradiance in the dam faces are non-uniform
47 (Jin *et al.* 2010). Solar energy requires a special treatment, since irradiance varies
48 throughout the day and year, and the incident angle of sunbeams varies across the faces
49 of arch dams due to a three-dimensional curvature and shadows, avoiding the incidence
50 of sunbeams.

51 The wide variety of inclination and azimuth angles of arch dam surfaces requires use of
52 models to compute the components of the irradiance - direct, diffuse and reflected - on
53 inclined surfaces. The diffuse component is composed of three parts (Duffie and
54 Beckman 2013): the isotropic component, circumsolar component and horizon
55 brightening component. The main difference between models lies in the treatment of the
56 diffuse component. The simplest approaches only consider an isotropic component,
57 such as the isotropic sky model (Liu and Jordan 1960) or those offered by Badescu
58 (Badescu 2002). Other techniques overlook the horizontal brightening component, such
59 as the Hay-Davies model (Duffie and Beckman 2013). The most complex models take
60 into account the three components, namely the Reindl (Reindl *et al*. 1990), Muneer
61 (Muneer 2004) and Perez (Perez *et al.* 1987) models. Comparisons and applications to
62 specific regions across the world have been reported, such as in Iran (Noorian *et al.*
63 2008), Spain (Diez-Mediavilla *et al.* 2005) or Saudi Arabia (El-Sebaii *et al*. 2010).

For a fixed surface, the incident angle of sunbeams and the position of shadow areas vary as the day progresses and should be computed, at least, hourly. If hourly solar irradiance is not measured at the site of interest, several approaches for estimating mean hourly global irradiance from daily global data on horizontal surfaces have been proposed. The first models, such as the Lui and Jordan model (Liu and Jordan 1960), assume that global radiation follows the same hourly distribution as that for extraterrestrial radiation. Later, some atmospheric effects as the hourly attenuation were also considered by means of empirical expressions, such as the Collares-Pereira and Rabl model (Collares-Pereira and Rabl 1979). Other techniques have improved accuracy by adding solar elevation as an input (Soler and Gopinathan 1994), such as the Gueymard model (Gueymard 2000). Several works provide comparisons between the performance of the previous models by using data from different locations in the word, as from the UK (Tham et al. 2010), India (Jamil Ahmad and Tiwari 2008) or worldwide (Gueymard 2000). The above mentioned works concluded the Gueymard model generally gives the best estimations.

Since solar radiation is computed on tilted surfaces, knowledge of irradiance components is required though these magnitudes are not sometimes available. Some models can be used for estimating hourly direct and diffuse irradiance from hourly global data. These involve two types: the radiative transfer and decomposition models (Batlles *et al*. 2000). Whereas the first require detailed information of atmospheric parameters, the second establish empirical correlations between the components of the irradiance, such as those offered by Liu and Jordan (Liu and Jordan 1963), the Reindl (Reindl *et al.* 1990) and the CLIMED2 (De Miguel *et al.* 2001) models.

Several approaches have been proposed for computing the temperature field in concrete dams under an operational life stage. Certain assumptions are considered in all works:

89 such as hydration heat generation being negligible, except during the construction phase
90 (Myers *et al*. 2009; Ulm and Coussy 2001; Briffaut *et al.* 2011; 2012), and concrete
91 being an isotropic material with constant thermal properties. Analytical and numerical
92 solutions of Fourier's law have been performed. Whereas analytical models require
93 prior knowledge of the dam faces, numerical techniques adopt a boundary condition of
94 imposed flux in the downstream face where heat fluxes are calculated as the sum of the
95 energy due to convection and electromagnetic radiation exchange between the dam and
96 the surrounding air and solar energy. A boundary condition of imposed temperature
97 equal to water temperature is used in the upstream face.

98 Stucky and Derron (1957) proposed an analytical one-dimensional solution for studying
99 heat transfer across a horizontal section of a dam. Temperatures of the faces were
100 assumed to follow a sinusoidal law in-phase and the solution extended to periodic but
101 non-harmonic temperatures in the faces by using a frequency domain solution (Léger
102 and Leclerc 2007).

103 Agullo *et al.* (1996) computed the concrete temperature field with a one-dimensional
104 numerical model based on an explicit finite difference scheme. Hourly irradiance
105 components were estimated by the Liu and Jordan model and diffuse components on
106 tilted surfaces by the isotropic sky model.

107 Leger *et al*. (1993a, 1993b) proposed a two-dimensional numerical approach for
108 computing thermal field in a gravity dam. Shades were not taken into account and
109 components of irradiance on tilted surfaces were computed by the isotropic sky model.
110 In a further study, Daoud, *et al.* (1997) then developed this work. Snow cover,
111 temperature gradients, ice formation in the reservoir water and conductivities for the
112 saturated and unsaturated parts of the dam were also taken into account.

Sheibany and Ghaemian (2006) studied the effects of thermal load over the stress field in the Karaj arch dam in Iraq. Foundation was not modeled, as the heat flow exchange between the dam and the foundation was not considered. Global irradiance data were obtained at a weather station situated nearby, components of solar radiation on a horizontal surface deduced by the authors and hourly solar radiation distribution estimated by the Collares-Pereira and Rabl model (Collares-Pereira and Rabl 1979).

Jin *et al*. (2010) proposed a procedure for predicting temperature on the exposed faces of arch dams. The foundation was modeled and the methodology validated with a case study. As solar radiation data were not available, irradiance was estimated with a model calibrated with an inverse thermal analysis. Only the isotropic component of the diffuse irradiance was considered.

Thermal studies are also carried out in other concrete structures. Bentz (2000) developed a one dimensional model to predict the surface temperature and time of wetness and freezing of concrete pavements and bridge decks. The domain was a vertical line from the top of the deck to the bottom. Boundary condition at the top of the deck are of imposed heat flux due to solar radiation, convection and the emitted radiation by the deck. The night cooling phenomena was considered, although neither shading nor evaporative cooling were accounted for. The model was employed for assessing techniques to increase the service life of concrete structures exposed to winter environment. One of those methods is to incorporate phase change materials which reduce the number or intensity of freeze thaw cycles (Bentz and Turpin 2007, Sakulich and Bentz 2012a, 2012b). Temperatures also have effects on the modal properties of some bridges (Liu and DeWolf 2007) and their defections (Roberts-Wollman et al. 2002).

Thermal studies also play a vital role in the modeling of the mechanical behavior of concrete at early ages. Wojcik et al. (2003) developed an energy balance model for forecasting temperatures and moisture of curing concrete bridge decks. Boundary conditions were imposed heat fluxes due to convection, radiation, evaporation of water, runoff water and concrete hydration. The model was employed for studying the sensitivity of concrete temperatures and moisture to atmospheric and construction conditions.

Faria et al. (2006) presented a methodology for the thermo-mechanical analysis of concrete at early ages. The methodology accounts for the evolution of the cement hydration reaction and the thermal and stress fields. The methodology was applied to a restrained reinforced concrete floor slab of a storage building which was monitored during its construction. Since the slab was indoor, solar radiation was not considered.

Azenha and Faria (2008) presented a numerical prediction of temperatures and stresses on a reinforced concrete foundation of a steel wind towel during concrete hydration and the first weeks after casting. Solar radiation and convection heat exchange were accounted for in the thermal model by adopting a constant convection-radiation coefficient.

Boutillon et al. (2012) analyzed the effects of sun radiation on temperature and stress distributions in early age concrete structures. A concrete beam was built outdoor and its temperature and stress fields during the curing process were computed by a thermo-hydro-chemo-mechanical model. Sun irradiation involves higher and sooner peak concrete temperature.

In this paper, a methodology for computing heat fluxes across the faces of arch dams during service located in the Iberian Peninsula is proposed. A detailed methodology for

161 computing heat fluxes due to the incident solar radiation over the dam faces is reported.
162 Moreover, the methodology accounts for the phenomena of night cooling and
163 evaporative cooling. The procedure is validated by using data from a case study: the La
164 Baells arch dam. The proposed methodology is compared with other simplified
165 approaches and the effect of solar radiation over the thermal field of the dam is also
166 analyzed. The consequences of the different approaches for computing the thermal field
167 on stress and displacement calculations are studied.

168 ## METHODOLOGY.

169 Heat transfer through the dam and its foundation is governed by the heat diffusion
170 equation expressed in Cartesian coordinates in a three-dimensional continuum isotropic
171 medium with no energy generation and constant properties -thermal conductivity λ,
172 density ρ and specific heat c- as (Incropera *et al*. 2011):

$$\frac{\lambda}{\rho c}\left(\frac{\partial^2\theta}{\partial x^2}+\frac{\partial^2\theta}{\partial y^2}+\frac{\partial^2\theta}{\partial z^2}\right)=\frac{\partial\theta}{\partial t} \quad (1)$$

173 where t is the time and θ the temperature. Thermal and mechanical properties of
174 concrete are assumed to be invariant with temperature as they diverge in a narrow range
175 (255-310 ºK) (Leger *et al*. 1993a, 1993b).

176 Boundary conditions are of imposed heat flux q in the dam faces in contact with air -
177 Fig. 1-, which may be expressed by Eq.(2). Heat fluxes due to solar radiation are not
178 considered in those parts of the valley where vegetation grows. Since the temperature of
179 the water-dam face is a complex problem, previous works have assumed that concrete
180 temperature is the same as that of the water in contact with it (Leger *et al.* 1993a).
181 Consequently, a temperature equal to water temperature is imposed in the dam faces
182 under water level. Infinite boundary elements for modeling the exterior infinite domain

183 are used in side surfaces where the foundation is truncated, i.e., in the surfaces which
184 limit the considered portion of the foundation.

$$-\lambda \frac{\partial \theta}{\partial t} = q \tag{2}$$

185 **Heat fluxes.**

186 The dam faces and the temporal domain are discretized in a finite number of sub-
187 domains. The upstream dam face Γ_u and downstream face Γ_d are divided into *K* areas,
188 respectively. The k^{th} area or sub-domain is denoted as Γ_k. The part of Γ_k exposed to
189 sunbeams is called $\Gamma_{s,k}$. The temporal domain is divided into *I* days and each day into *J*
190 intervals. The heat flux in the k^{th} area at the j^{th} time in the i^{th}day is denoted as $q_{i,j,k}$.
191 Heat fluxes are considered to be uniform at every spatial and temporal sub-domain. An
192 example of spatial discretization is shown in Fig. 2.

193 Heat fluxes across the dam faces in contact with air in the k^{th} area at the j^{th} time in the
194 i^{th}day $q^{i,j,k}$ are the sum of the energy due to convection$q_c^{i,j,k}$, long wave radiation
195 exchange $q_r^{i,j,k}$, solar energy and $q_s^{i,j,k}$ and evaporative cooling $q_{ev}^{i,j,k}$, defined as:

$$q^{i,j,k} = q_c^{i,j,k} + q_r^{i,j,k} + q_s^{i,j,k} + q_{ev}^{i,j,k} \tag{3}$$

196 Convection between the dam surface and the air is a complex phenomenon which is
197 influenced by many variables, such as the shape and the rogosity of the surface or wind
198 speed. Convective heat exchange is governed by Newton's Law of Cooling. Heat flow is
199 proportional to the difference between dam face temperature and the ambient
200 temperature θ_a Eq.(4),

$$q_c^{i,j,k} = h^{i,j,k}\left(\theta_a^{i,j,k} - \theta^{i,j,k}\right) \quad (4)$$

where $h^{i,j,k}$ is the convection coefficient.

A widely diversity of experimental formulae for assessing h have been proposed (Palyvos 2008). Correlations proposed by Kehlbeck have provided accurate results in application to concrete box girder bridges (Mirambell and Aguado 1990) and dams (Agullo *et al*. 1996). The coefficient h in $Wm^{-2}°C^{-1}$ is computed by Eq.(5) in the outer surfaces, where forced convection is presented and wind speed has a V_w value in m/s, and by Eq.(6) in the inside surfaces where convection is natural.

$$h^{i,j,k} = 3.67 + 3.83V_w^{i,j,k} \quad (5)$$

$$h^{i,j,k} = 3.5 \quad (6)$$

Long wave radiation exchange is modeled through the Stefan-Boltzmann law, expressed by Eq.(7) in which e is the emissivity of the concrete surface, C_s is the Stefan-Boltzmann constant and $\theta_s^{i,j}$ is the sky temperature.

$$q_r^{i,j,k} = eC_s\left(\left(\theta_{sk}^{i,j}\right)^4 - \left(\theta^{i,j,k}\right)^4\right) \quad (7)$$

During the day, the sky temperature can be considered to be equal to the ambient temperature. However, during the night the sky temperature can be lower than the ambient. This phenomenon is called night cooling. Chen et al. (1995) proposed the empirical expression given by Eq.(8) for computing the emissivity of the sky e_{sk}. The sky temperature is then assessed by Eq.(9).

$$e_{sk} = 0.736 + 0.00577\theta_{dp} \quad (8)$$

$$\theta_{sk} = (e_{sk})^{0.25}\theta_a \quad (9)$$

216 θ_{dp} is the dew point temperature which is computed by the Clausius-Clapeyron
217 equation as a function of the relative humidity and the ambient temperature (Lawrence,
218 2005).

219 The evaporative cooling $q_{ev}^{i,j,k}$ is a heat loss due to the evaporation of water on the dam
220 surfaces. Water comes from rainfall in dams during service life. $q_{ev}^{i,j,k}$ is computed by
221 Eq.(10), where $q_m^{i,j,k}$is the moisture evaporative flux in kgs^{-1} and h_t is the latent heat of
222 evaporative water in Jkg^{-1}.

$$q_{ev}^{i,j,k} = -q_m^{i,j,k} h_t^{i,j} \quad (10)$$

$$h_t = 2500 \cdot 10^3 - 2500(\theta_a - 273.15) \quad (11)$$

223 $q_m^{i,j,k}$ is computed by Eq.(12), where E_s is the moisture emissivity coefficient in
224 $kgm^{-2}s^{-1}Pa^{-1}$, e_s is the saturation vapour pressure in Pa and H_r is the relative
225 humidity. e_s can be calculated by the Clausius-Clapeyron equation (Lawrence, 2005).

226

$$q_m^{i,j,k} = E_s^{i,j,k} e_s^{i,j,k}\left(1 - H_r^{i,j,k}\right) \quad (12)$$

227 E_s is defined by the Lewis' relationship, based on the similarity approach of the
228 boundary layer theory (Incropera et al. 2011). The relationship can be approximately
229 computed as (Chuntranuluck et al. 1998):

$$\frac{h}{E_s} \approx \frac{29\, c_s P}{18} \quad (13)$$

230 where h is the convection coefficient, c_s is the specific heat capacity of air (1007
231 $Jkg^{-1}K^{-1}$) and P is the total air pressure in Pa.

Heat flow due to solar irradiation requires special treatment as the magnitude of the solar irradiance and its incident angle over the dam surfaces are not constant during the day. Moreover, the magnitudes of the solar radiation components depend on the orientation and slope of the surface and shading. Consequently, assessment of the heat flux is a complex process whose steps are described below.

Solar radiation components on horizontal surfaces.

Hourly global solar irradiation data on a horizontal surface should be required. Although this data is not usually measured in the location of interest, it may be estimated. Gueymard (2000) proposed a model which provides the ratio r_t between the mean hourly global insolation I_G and the daily global insolation H_G for the middle point on each hourly period. r_t is provided as a function of the extraterrestrial hourly/daily insolation ratio r_o corrected by several coefficients and the empirical expressions a_1 and a_2.

The coefficients consider the influence of latitude ϕ, solar declination δ, solar hour angle ω and sunrise hour angle ω_o. The expressions a_1 and a_2 correct r_t from the atmospheric effects and both are polynomial functions of the clearness index K_t, the daily-average solar elevation outside of the atmosphere α_o and the day length in hours S_o. K_t is the ratio of H_G to the extraterrestrial daily global irradiance on a horizontal surface, $H_{G,o}$. The coefficients are determined by a multiple least-squared fit using data from 135 radiation sites around the world. Expressions for estimating δ, $H_{G,o}$, ω_o, ω and S_o are provided in Appendix A.

$$r_o = \frac{I_G}{H_G} = \frac{\pi}{24}\left[\frac{\cos\omega - \cos\omega_o}{\sin\omega_o - \omega_o\cos\omega_o}\right] \quad (14)$$

$$r_t = r_o \left[\frac{1 + \cos\phi \cos\delta \left(\frac{a_1}{a_2}\right) (\cos\omega - \cos\omega_o)}{1 + \cos\phi \cos\delta \left(\frac{a_1}{a_2}\right) \frac{\omega_o (0.5 + \cos^2\omega_o) - 0.75 \sin 2\omega_o}{\sin\omega_o - \omega_o \cos\omega_o}} \right] \quad (15)$$

253

$$a_1 = 0.41341 K_t + 0.61197 K_t^2 - 0.01886 K_t S_o + 0.00759 S_o$$

$$a_2 = Max(0.054, 0.28116 + 2.2475 K_t - 1.76118 K_t^2 \quad (16)$$

$$- 1.84535 \sin\alpha_o + 1.6811 \sin^2\alpha_o)$$

254 Once hourly global insolation on a horizontal surface is known, insolation is
255 decomposed into the beam and the diffuse hourly components on horizontal surfaces.
256 For that purpose, a decomposition model especially suitable for the area in interest was
257 used.

258 The hourly correlation CLIMED2 (De Miguel *et al.* 2001) provides an empirical
259 relationship between the hourly diffuse fraction k_d and the hourly global clearness
260 index k_t given by Eq.(17). k_d is defined as the ratio of the hourly diffuse insolation to
261 the hourly global insolation and k_t is the ratio of the hourly global insolation to the
262 extraterrestrial hourly global insolation. The coefficients of Eq.(17) were determined by
263 using data from radiation sites located in the North Mediterranean belt area, including
264 sites from France, Greece, Portugal and Spain.

$$k_d = 0.995 - 0.081 k_t \quad \text{for } k_t \leq 0.21$$

$$k_d = 0.724 + 2.738 k_t - 8.320 k_t^2 + 4.967 k_t^3 \quad \text{for } 0.21 < k_t \leq 0.76 \quad (17)$$

$$k_d = 0.180 \quad \text{for } k_t > 0.76$$

265 **Shading.**

Shading on dam faces is computed at each central temporal interval by means of a vector approach based on descriptive geometry. The shadow projection of a point onto the surface Γ is given by the intersection of the straight line having the sunbeams direction and that passes through the considered point. Cast shadows are evaluated by repeating the procedure for all points in the domain which can produce shading. Sunbeam directions at the desired time are assessed by the solar angles altitude α and azimuth ψ, computed with the expressions included in Appendix A.

Dam faces are defined by parabolic curves in a Cartesian coordinate system (O, xyz) with an origin O that lies in the upstream edge of the crown cantilever crest. The x and y axes lie in a horizontal plane. The x-axis is drawn to the left abutment, the y-axis downstream and the z-axis vertically downward. The downstream face Γ_d is defined by Eq.(18) and the upstream face Γ_u by Eq.(19):

$$\Gamma_d: y(x,z) = \frac{1}{2r_d(z)}x^2 + b(z) + t_c(x) \tag{18}$$

$$\Gamma_u: y(x,z) = \frac{1}{2r_u(z)}x^2 + b(z) \tag{19}$$

where r_d and r_u are the radii of curvatures of the downstream and upstream horizontal arch curves, b is a function which defines the upstream face of the crown cantilever and t_c is the thickness of the crown cantilever. r_d, r_u, b and t_c are obtained from:

$$r_d(z) = n_1(z)r_{d1} + n_2(z)r_{d2} + n_3(z)r_{d3} \tag{20}$$

$$r_u(z) = n_1(z)r_{u1} + n_2(z)r_{u2} + n_3(z)r_{u3} \tag{21}$$

$$b(z) = -sz + \frac{sz^2}{2\varphi H} \tag{22}$$

$$t_c(z) = n_1(z)t_{c1} + n_2(z)t_{c2} + n_3(z)t_{c3} \tag{23}$$

in which z is the axis vertically downward, r_{d1}, r_{d2}, r_{d3}, r_{u1}, r_{u2} and r_{u3} are, respectively, the values of r_d and r_u at $z = 0$, $z = \zeta H$ and $z = H$, s is the slope of the crown cantilever at the crest, H is the height of the crown cantilever, φ is the relative height ($\varphi = z/H$) at which the slope of the crown cantilever is zero, t_{c1}, t_{c2} and t_{c3} are, respectively, the thickness of the crown cantilever at $z = 0$, $z = \zeta H$ and $z = H$. n_1, n_2 and n_3 are quadratic functions defined as:

$$n_1(z) = \frac{\left(\frac{z}{H} - \zeta\right)\left(\frac{z}{H} - 1\right)}{\zeta} \tag{24}$$

$$n_2(z) = \frac{\left(\frac{z}{H}\right)\left(\frac{z}{H} - 1\right)}{\zeta(\zeta - 1)} \tag{25}$$

$$n_3(z) = \frac{\left(\frac{z}{H}\right)\left(\frac{z}{H} - \zeta\right)}{1 - \zeta} \tag{26}$$

The points to be considered when computing the limit of shading at each hour are the edges of the abutments, which define the shadows cast by the riversides onto the dam, and the edges of the crown cantilever and the tangent points in the dam surfaces to sun rays which define the shadows cast by the dam onto itself and the valley. Given a unit vector parallel to sun ray $\vec{\mathrm{r}} = (\mathrm{r_x}, \mathrm{r_y}, \mathrm{r_z})$ defined in the $(\mathrm{O}, \mathrm{xyz})$ Cartesian system, the projection of the edge in the abutments onto the downstream dam face is given by Eq.(27) and onto the upstream face by Eq.(28):

$$\begin{cases} \mathrm{x} = \dfrac{\mathrm{r_x}}{\mathrm{r_z}}\xi + \mathrm{x_r} \\ \mathrm{y} = \dfrac{1}{2\mathrm{r_d}(\xi)}\left(\dfrac{\mathrm{r_x}}{\mathrm{r_z}}\xi + \mathrm{x_r}\right)^2 + \mathrm{b}(\xi) + \mathrm{t_c}(\xi) \\ \mathrm{z} = \xi \end{cases} \tag{27}$$

$$\begin{cases} x = \dfrac{r_x}{r_z}\xi + x_r \\ y = \dfrac{1}{2r_u(\xi)}\left(\dfrac{r_x}{r_z}\xi + x_r\right)^2 + b(\xi) \\ z = \xi \end{cases} \tag{28}$$

where $\mathbf{x_r}$ is the distance between the origin **O** and the edge.

The projection of the upstream edge of the crown cantilever onto the upstream dam face is given by the intersection of two surfaces. The first one is the projection of the upstream edge of the crown cantilever and the second is the upstream dam face, both given by Eq. (29). The projection of the downstream edge of the crown cantilever onto the downstream dam face is computed in the same manner by Eq. (30). Points in the upstream edge of the crown cantilever cannot be projected onto downstream face and vice versa, as rays are obstructed by the dam.

$$\begin{cases} y = \dfrac{r_y}{r_z}z + \dfrac{1}{2r_{u1}}\left(x - \dfrac{r_x}{r_z}z\right)^2 \\ y = \dfrac{1}{2r_u(z)}x^2 + b(z) \end{cases} \tag{29}$$

$$\begin{cases} y = \dfrac{r_y}{r_z}z + \dfrac{1}{2r_{d1}}\left(x - \dfrac{r_x}{r_z}z\right)^2 \\ y = \dfrac{1}{2r_d(z)}x^2 + b(z) + t_c(z) \end{cases} \tag{30}$$

The points where the sun rays are tangent to the upstream dam face define a shadow area, bordered by these points and the foundation. Points tangent to sun rays are found by ascertaining that the normal vectors to dam surface are perpendicular to sun rays. Therefore, Eq(31) must be satisfied.

$$\nabla\Gamma_u \cdot \vec{r} = 0 \tag{31}$$

Since these points belong to the dam face, they are computed by the intersection of the two surfaces as follow:

$$\begin{cases} \dfrac{\partial \mathrm{r_u(z)}}{\partial \mathrm{z}} \dfrac{\mathrm{r_z}}{2\mathrm{r_u(z)}^2}\mathrm{x}^2 - \dfrac{\mathrm{r_x}}{\mathrm{r_u(z)}}\mathrm{x} - \dfrac{\partial \mathrm{b(z)}}{\partial \mathrm{z}}\mathrm{r_z} + \mathrm{r_y} = 0 \\ \mathrm{y} = \dfrac{1}{2\mathrm{r_u(z)}}\mathrm{x}^2 + \mathrm{b(z)} \end{cases} \quad (32)$$

Solar radiation components & heat fluxes across dam faces.

The components of the global hourly insolation on a tilted surface, $I_{T,G}$, are driven by the Reindl model (Reindl *et al*. 1990) which provides accurate estimates in Spain (Diez-Mediavilla *et al.* 2005). The total insolation on a tilted surface is the sum of three components: the beam $I_{T,b}$, the diffuse $I_{T,d}$ and the reflected radiation from the ground to the surface $I_{T,g}$. The diffuse insolation involves three parts: the isotropic $I_{T,d,iso}$, the circumsolar $I_{T,d,cs}$ and the horizon brightening $I_{T,d,hb}$. The total insolation on the k^{th} area of the dam face at the j^{th} local apparent hour in the i^{th}day is given by Eq.(33).

$$I_T^{i,j,k} = I_{T,b}^{i,j,k} + I_{T,d,cs}^{i,j,k} + I_{T,d,iso}^{i,j,k} + I_{T,d,hb}^{i,j,k} + I_{T,g}^{i,j,k} \quad (33)$$

The components of total radiation are expressed in terms of the beam and diffuse insolation on a horizontal surface. The Reindl model is expressed as follow:

$$\begin{aligned} I_T = I_b R_b + I_d A R_b \; + I_d(1-A)\left(\frac{1+\cos\beta}{2}\right) \\ + I_d(1-A)\left(\frac{1+\cos\beta}{2}\right)\left(\sqrt{\frac{I_b}{I_G}}\sin^3\frac{\beta}{2}\right) + I_G g_r\left(\frac{1-\cos\beta}{2}\right) \end{aligned} \quad (34)$$

where R_b is the ratio of beam insolation on the tilted surface to that on a horizontal surface at any time, A is the anisotropy index, β is the slope of the tilted surface and g_r is the ground refrectivity.

The anisotropy index A, defined in Eq.(35), accounts for the portion of the diffuse insolation treated as circumsolar -$I_d A$-, and consequently, with anisotropic nature. It is considered to be incident at the same angle as the beam radiation. The index is the

relationship between the hourly beam insolation on a horizontal surface I_b and the hourly extraterrestrial irradiation on a horizontal surface $I_{G,o}$. The remaining portion is assumed to be isotropic.

$$A = \frac{I_b}{I_{G,o}} \tag{35}$$

Since areas of the dam surface are not completely flat due to a double curvature of arch dams, the total insolation on the k^{th} area of the dam face at the j^{th} local apparent hour in the i^{th}day is expressed in differential terms as follows:

$$I_T^{i,j,k} = I_{n,b}^{i,j} \frac{\iint_{\Gamma_{s,k}} \left(\overrightarrow{r^{i,j}} \cdot \vec{n}\right) d\Gamma_{s,k}}{\iint_{\Gamma_k} d\Gamma_k} + I_d^{i,j} A^{i,j} \frac{\iint_{\Gamma_{s,k}} \left(\overrightarrow{r^{i,j}} \cdot \vec{n}\right) d\Gamma_{s,k}}{\iint_{\Gamma_k} d\Gamma_k} + I_d^{i,j} \big(1 -$$

$$A^{i,j}\big) \frac{\iint_{\Gamma_k} \left(\frac{1+\vec{n}\cdot\vec{k}}{2}\right) d\Gamma_k}{\iint_{\Gamma_k} d\Gamma_k} + I_d^{i,j} \left(1 - A^{i,j}\right) \sqrt{\frac{I_b^{i,j}}{I_G^{i,j}}} \frac{\iint_{\Gamma_k} \left(\frac{1+\vec{n}\cdot\vec{k}}{2}\right)\left(\frac{1-\vec{n}\cdot\vec{k}}{2}\right)^{3/2} d\Gamma_k}{\iint_{\Gamma_k} d\Gamma_k} + \tag{36}$$

$$I_G^{i,j}\, g_r^{i,j,k} \frac{\iint_{\Gamma_k} \left(\frac{1-\vec{n}\cdot\vec{k}}{2}\right) d\Gamma_k}{\iint_{\Gamma_k} d\Gamma_k}$$

where $\vec{n}$ is the unit normal vector to dam surface, $\vec{k}$ is the unit vector directed toward the north celestial pole and $\overrightarrow{r^{i,j}}$ is the unit vector parallel to sun ray at the j^{th} local apparent hour in the i^{th}day. The anisotropic components of the solar radiation are considered as a vector field whose direction is parallel to sun rays and modulus is equal to $I_{n,b} + I_d A$. The incident solar radiation on the considered area due to the anisotropic components is computed by the surface integral of that vector field over the considered area. The remaining components of the radiation are function of the angle β, which varies with the position in the area. Therefore, mean values of the terms depending on the angle are computed in differential terms.

Heat fluxes across the k^{th} area of the dam face at the i^{th}day are given by:

$$q_c^{i,k} = \sum_{j=1}^{J} q_c^{i,j,k} \;;\; q_r^{i,k} = \sum_{j=1}^{J} q_r^{i,j,k} \;;\; q_{ev}^{i,k} = \sum_{j=1}^{J} q_{ev}^{i,j,k} \;;\; q_s^{i,k} = a_k \sum_{j=1}^{J} I_T^{i,j,k} \qquad (37)$$

where a_k is the solar absorptivity of the considered area. Total heat transfer across the k^{th} area at the i^{th}day is then calculated as:

$$q^{i,k} = q_c^{i,k} + q_r^{i,k} + q_{ev}^{i,k} + q_s^{i,k} \qquad (38)$$

Simplified method for computing heat fluxes.

Some simplified procedures for computing heat fluxes have been proposed. One of them is denoted as "sol-air temperature", which is the ambient temperature that in the absence of all radiation changes provides the same rate of heat flow as would the sum of incident solar radiation, convection heat flow and long wave radiation exchange (ASHRAE 2001). The sol-air temperature at the j^{th} local apparent time in the i^{th}day $\theta_e^{i,j}$ is given by:

$$\theta_e^{i,j} = \theta_a^{i,j} + \frac{\alpha I_T^{i,j}}{h_o} - \frac{e\Delta R^{i,j}}{h_o} \qquad (39)$$

where h_o in $Wm^{-2}K^{-1}$ is the coefficient of heat transfer by long wave radiation and convection and $\Delta R^{i,j}$ in Wm^{-2} is the different between the long wave radiation incident on the dam face from sky and surroundings and radiation emitted by blackbody at ambient temperature. The heat flow is then expressed as:

$$q^{i,j} = h_o\left(\theta_e^{i,j} - \theta^{i,j}\right) \qquad (40)$$

A common practice is to assume $e\Delta R = 0$ for vertical surfaces and $\Delta R = 63\ Wm^{-2}$ for horizontal surfaces. Moreover, the ratio α/h_o is equal to 0.026 for a light colored surface and 0.052 for dark colored (ASHRAE 2001).

As the sol-air temperature model is a quick and straightforward method for computing heat fluxes, a simplified geometry of the dam will be adopted when calculating incident solar radiation. The curvature of the dam faces will be neglected and the structure will be resembled to a flat vertical wall. If the curvature is accounted for, incident solar radiation has to be assessed by the proposed methodology and the simplicity of the sol-air method would be lost.

Water temperature.

A boundary condition of imposed temperature is used in the parts of the dam faces under water level, where concrete temperature is assumed to be equal to water temperature. Water temperature can be estimated by means of hydrothermal models based on the first law of thermodynamics and on the heat transfer relationships. Other approaches combine computational fluid dynamic and heat transfer models (Yu and Wang 2011). However, these approaches are complex and computationally intense. Analytical models, which are an alternative with a straightforward and simple formulation, are composed of several algebraic terms and parameters which may be provided or estimated with water temperature observations at the site of interest.

In this work, the water temperature θ_w at day t and deep z is computed by Bofang model (Bofang 1998), which is an analytical model of the form:

$$\theta_w(z,t) = \left(\frac{\overline{\theta_{w,b}} - \overline{\theta_{w,s}}e^{-0.04H}}{1-e^{-0.04H}}\right) + \left(\overline{\theta_{w,s}} - \frac{\overline{\theta_{w,b}} - \overline{\theta_{w,s}}e^{-0.04H}}{1-e^{-0.04H}}\right)e^{-0.04H} + A_{w,s}e^{-0.018z}\cos\left(\omega_w\left(t - t_o - 2.15 + 1.30e^{-0.085z}\right)\right) \quad (41)$$

where $\overline{\theta_{w,b}}$ is the mean annual water temperature at the bottom of the reservoir, $\overline{\theta_{w,s}}$ is the mean annual water temperature at the surface, H is the depth of reservoir, $A_{w,s}$ is the annual water temperature amplitude at the surface, ω_w is the angular frequency of the

water temperature cycle -assumed to be equal to $2\pi/365$ days^{-1}- and t_o is the day at which ambient temperature is maximum. Values of the previous variables are provided for lakes and reservoirs in China. The magnitude of the unknown variables can also be estimated by using water temperature observations at the reservoir of interest.

The finite element model.

Thermal analyses

The discretized governing equation Eq.(1) at time $\mathrm{t_n}$ leads to the following system of expressions:

$$[\mathbf{C}]\{\dot{\boldsymbol{\theta}}_{\mathrm{n}}\} + [\mathbf{K_T}]\{\boldsymbol{\theta}_{\mathrm{n}}\} = \{\mathbf{F_T}\} \tag{42}$$

where $[\mathbf{C}]$ is the specific heat matrix, $[\mathbf{K_T}]$ is the conductivity matrix, $\{\mathbf{F_T}\}$ is the vector of applied heat flows, $\{\boldsymbol{\theta}_{\mathrm{n}}\}$ is the vector of nodal temperatures at time $\mathrm{t_n}$ and $\{\dot{\boldsymbol{\theta}}_{\mathrm{n}}\}$ is the time rate of the nodal temperature values at time $\mathrm{t_n}$. Eq.(42) is solved by the generalized trapezoidal rule (Hughes 2000), which yields to:

$$\{\boldsymbol{\theta}_{\mathrm{n+1}}\} = \{\boldsymbol{\theta}_{\mathrm{n}}\} + (1-\vartheta)\Delta t\{\dot{\boldsymbol{\theta}}_{\mathrm{n}}\} + \vartheta\Delta t\{\dot{\boldsymbol{\theta}}_{\mathrm{n+1}}\} \tag{43}$$

where ϑ is a transient integration parameter. Substituting $\{\dot{\boldsymbol{\theta}}_{\mathrm{n+1}}\}$ from Eq.(43) into Eq.(42) at time $\mathrm{t_{n+1}}$ leads to:

$$\left(\frac{1}{\vartheta\Delta\mathrm{t}}[\mathbf{C}] + [\mathbf{K}]\right)\{\boldsymbol{\theta}_{\mathrm{n+1}}\} = \{\mathbf{F}\} + [\mathbf{C}]\left(\frac{1}{\vartheta\Delta\mathrm{t}}\{\boldsymbol{\theta}_{\mathrm{n}}\} + \frac{1-\vartheta}{\vartheta}\{\dot{\boldsymbol{\theta}}_{\mathrm{n}}\}\right) \tag{44}$$

providing a solution with nodal temperatures at time $\mathrm{t_{n+1}}$. Once $\{\boldsymbol{\theta}_{\mathrm{n+1}}\}$ is determined, $\{\dot{\boldsymbol{\theta}}_{\mathrm{n+1}}\}$ is updated using Eq.(43) and $\{\boldsymbol{\theta}_{\mathrm{n+2}}\}$ is computed by Eq.(44).

Structural analyses.

Structural analyses are carried out by solving the elasticity equations with the finite element method. Materials are assumed to be elastic and isotropic and have linear

396 properties. The discretized elasticity equations yield to the following system of linear
397 equations:

$$[K_S]\{D\} = \{F_S\} \quad (45)$$

398 where $\{D\}$ is the nodal displacement vector, $[K_S]$ is the stiffness matrix and $\{F_S\}$ is the
399 vector of applied forces. Thermal forces are generated by the difference between the
400 thermal strain and the thermal strain free produced by the reference thermal field which
401 occurs in the contraction joint grouting day.

402 CASE STUDY.

403 The case study is the La Baells dam which is a doubled-arch dam located on the
404 Llobregat River in the province of Barcelona. The dam is located at 42.1220º North
405 Latitude and 1.8785º East Longitude. The dam axis direction, from upstream to
406 downstream, is S0º E (South 0º East). It has a maximum height of 102 m, a crest length
407 of 403 m and a total reservoir volume of 115 hm^3. Its thickness varies from 4 m at the
408 crest to 20.1 m at the base. The dam faces are defined by parabolic curves.

409 There are 21 thermometers embedded in the concrete and five more installed in the
410 upstream face for recording water temperature. The situation of thermometers is
411 schematically illustrated in Fig. 3 and listed in Table 1. Wind speed, global solar
412 insolation, mean air temperature, relative humidity, rainfall, total air pressure and water
413 level in the reservoir are registered daily at the weather station installed in the dam
414 location. Data sets were available from 1 January 2006 to 31 July 2008. Concrete and
415 foundation properties are listed in Table 2 which were determined by laboratory tests
416 during the dam construction.

417 RESULTS AND DISCUSSION.

418 The proposed methodology for modeling thermal response of a concrete dam is applied
419 at the La Baells dam. The concrete temperature is determined by a finite element model
420 and the results are compared with the observations recorded in thermometers.

421 ## Heat fluxes.

422 The daily recording of air temperature, relative humidity, rainfall, total air pressure and
423 wind speed data led to a corresponding daily computation of heat fluxes due to
424 convection, long wave radiation exchange and evaporative cooling. Furthermore, air
425 temperature and wind speed were assumed to be spatially uniformly distributed over the
426 entirety of each face since these variables were only measured at the weather station
427 installed in the dam site. Assuming a constant wind speed along the dam involves a
428 constant convective coefficient which leads to a reduction of the spatial variability of
429 the concrete temperature at the dam faces. A rigorous wind speed study requires a
430 computational fluid dynamics model which is beyond the scope of the present study. As
431 these fluxes depended on the dam face temperature, they were assessed for temperatures
432 within the range of 270ºK-350 ºK every 10 ºK. Galleries were modeled by using
433 elements whose thermal properties were equal to the thermal characteristics of the air..

434 In order to compute solar heat flux, dam faces were divided into 570 areas: 19 in a
435 vertical direction, 12 in a horizontal direction at the base, and 48 at the crest. The areas
436 had a height of 6.3 m and a mean width of 5 m in the valley and 6 m in the abutments.
437 Time was divided hourly and global solar insolation estimated at every interval by Eq.
438 (14), (15) and (17) and the components then computed by means of Eq.(33).

439 Hourly insolation on every area was then computed by using Eq.(36). Ground
440 refrectivity was assumed to be equal to 0.250 in the downstream face and 0.125 in the

441 upstream face. The previous values corresponded respectively to wooded ground and
442 the water surface (Duffie and Beckman 2013).

443 Fig. 4 shows hourly insolation on 5 July 2007 on dam faces over two hourly intervals:
444 6:00 to 7:00 and 11:00 to 12:00. Shading at midpoint of the hourly interval is also
445 depicted in black lines. The downstream surface in the La Baells dam is south facing.

446 Shades over the downstream face at 6:30 -Fig. 4(a)- are caused by the upstream face
447 which prevents sunrays from striking the face and, consequently, results in only a small
448 area being exposed to sun rays. Limits are determined by the projection of the
449 downstream edge of the crown cantilever. Shades over the upstream face -Fig. (4b)- are
450 caused by the left abutment and the geometry of the face. The area exposed to sun rays
451 is defined by the projection of the left edge of the abutment and the points in the face
452 tangent to sun rays.

453 Shading at 11:30 is quite different from that before, given that the solar position
454 changes throughout the day. The downstream face -Fig. 4(c)- is exposed to sun rays,
455 except for a small area close to the top where the crest avoids rays striking the area. The
456 limits are computed by the projection of the downstream edge of the crest over the dam
457 face. A large part of the upstream surface -Fig. 4(d)- is shaded due to the shape of the
458 face, which prevents sun rays from reaching the lower part of the face because of sun
459 rays. Shading is limited by the points of the face tangent to sun rays

460 Insolation varies significantly across the dam faces, as shading prevents a percentage of
461 the solar radiation from reaching some parts of the surface. Furthermore, the double
462 curvature of the dam surface involves a wide variety of orientations and slopes which
463 make the total insolation vary at the points across the dam surface.

464 The shading effect over insolation is evaluated by studying two points located in the
465 upstream crow cantilever face in Fig. 4(b), at heights of 50 and 53 m respectively.
466 While both points have the same orientation and a similar slope, the first one is exposed
467 to the sunbeam and the second is in a shaded area. The degree of sun energy reaching
468 the points is 0.6 MJ/m^2 and 0.4 MJ/m^2 respectively. In this case, shading involves that
469 the energy which reaches the area is reduced a 33%.

470 The effects of the double curvature over insolation are analyzed by using Fig. 4(c). The
471 main part of the downstream face is subjected to sunbeams over 11:00 to 12:00. though
472 sun energy reaches the surface varies spatially. The areas close to the foundation receive
473 more energy than those at the crest. Energy varies from 2.0 MJ/m^2 at the point at the
474 base of the crown cantilever to 0.6 MJ/m^2 at the crest. While the points share the same
475 orientation, they have different slopes which cause a non-uniform distribution. The
476 point near to the base has a lesser degree of inclination than that close to the crest where
477 the cantilever is almost vertical. The effect of the orientation is appreciated when an
478 arch is analyzed, where points have similar slopes. Energy reaching the arch is higher in
479 the key than in the springing. However, insolation in Fig. 4(c) is skewed left (negative
480 x-axis) because the sun position is computed at 11:30. At that time, the areas in the left
481 side of crown cantilever capture more energy than those on the right side.

482 Insolation, upon reaching a given point, also varies during the day due to the variation
483 of the atmospheric conditions and the position of the sun, such as insolation when
484 reaching a point located at the crest of the upstream side close to the left abutment
485 (positive x-axis). Solar energy at 6:00 to 7:00 is equal to 1 MJ/m^2 - Fig. 4(b)- and at
486 11:00 to 12:00 is 1.5 MJ/m^2 - Fig. 4(d)- which involves an increase of 50%.

487 Daily insolation on 5 July 2007 at the downstream dam face is illustrated in Fig. 4(e).
488 Energy captured by the arches decreases with the topographic height increases due to

489 the slope of the areas. Areas near to the foundation of the crown cantilever have a slope
490 that favors capturing solar energy more than those close to the crest. The normal vectors
491 to the surface at the lower arches are oriented toward the zenith and the foundation at
492 the upper arches. Moreover, insolation is symmetric with respect to the crown cantilever
493 due to the dam orientation.

494 Daily insolation on the same day at the upstream face is depicted in Fig. 4(f). Insolation
495 is symmetrically distributed with respect to the crown cantilever. However, the energy
496 captured by arches increases, as does the topographic height (opposite to the
497 downstream face). The slope of the areas close to the crest is more likely to receive
498 solar radiation than the lower areas do.

499 The spatial distribution of insolation examined above corresponds to that of July. In the
500 upstream face, this distribution pattern is valid for other months too. However, some
501 differences are presented in the downstream face. The area exposed to sunbeams is
502 larger in winter than in summer because solar elevation is lower. Moreover, since the
503 downstream face is south oriented, it always captures more solar energy than the
504 upstream face.

505 Heat flux, due to solar radiation across every area of the dam faces each day, is
506 computed by Eq. (37). Solar absorptivity is assumed to be constant and its magnitude
507 determined during the calibration of the numerical model. A value of 0.75 was found to
508 provide the best estimations of concrete temperature. The value is within the range for
509 mature concrete with gray Portland cement (0.89-0.45) (Levinson and Akbari 2002).

510 Fig. 5(a) depicts the mean heat fluxes across the downstream face of the La Baells dam
511 due to solar radiation, convection and electromagnetic radiation exchange between the
512 dam and the air. Fluxes are determined once the concrete temperature is computed by
513 the numerical model. Fig. 5(b) illustrates the downstream face temperature evolution.

514 The mean daily face temperature is plotted, together with the maximum and the
515 minimum face temperatures, as well as the mean air temperature.

516 Solar radiation constantly generates a positive flux; that is to say, the heat flows into the
517 dam which involves an increase of the concrete temperature, and evaporation a negative
518 flux. In addition, the minimum downstream face temperature is often greater than the
519 mean air temperature. As a result, convective and radiative heats flow out of the dam,
520 cooling the concrete and acting as a thermal regulator. An exception was found on 22
521 November 2007 when air temperature rose after several cold days. On this occasion, the
522 downstream face temperature was lower than the ambient temperature and the three heat
523 sources flow into the dam, with the consequence being a heating of the concrete.

524 The sum of the four heat flow sources is plotted in Fig. 5(c). The significant degree of
525 variability of solar radiation, air temperature, evaporation and wind speed produces a
526 noisy total flux which, consequently, impede appreciation of its stationary pattern. For
527 this reason, a smoothed flux with a moving average is depicted in a solid black line.

528 Energy flows into the dam from mid-spring to the end of summer, heating the concrete,
529 with the solar heat flow being greater than the other flows. During the remaining days
530 of the year, heat flows outside because the solar radiation reaching the dam decreases
531 and air temperature drops. Convection, evaporation and radiative heats, which tend to
532 cool the concrete as shown in Fig. 5(a), are greater than solar energy and the dam
533 temperature decreases.

534 ## Water temperature.

535 The water temperature at the La Baells reservoir is measured by means of five water
536 thermometers installed at the upstream face of the dam. Parameters of the Bofang model
537 were estimated by the least squared method by using the recorded data. The mean

annual water temperature at the surface of the reservoir is 15.19 ºK and at the bottom 9.33 ºK. The annual water temperature amplitude at the surface is 6.51 ºK and the ambient temperature is at a maximum on the 201st day of the year. The observations are estimated with a root mean square equal to 2.52 ºK and a negligible bias.

The water temperature in other points and dates was estimated by means of the Bofang model. Fig. 6 depicts the evolution of the water temperature at several depths. As depth increases, the amplitude and the mean temperature of the water decreases because of the attenuation of the atmospheric effects.

The finite element model.

Thermal analyses.

The heat diffusion equation is solved in the domain by the finite element method with a one-day time step. The domain composes the arch dam and a finite region of its foundation, with both being discretized with eight-node cubic elements. The dam domain is composed of 54,666 elements with 56,100 nodes and the foundation domain of 53,939 elements with 54,014 nodes (thermal and mechanical properties are listed in Table 2. The adopted mesh is shown in Fig. 7(a) and a detail of the central crown cantilever in the Fig. 7(b).

Initial consistent temperatures at nodes should be specified at the first load step. The initial temperatures were computed by the analytical solution proposed by Stucky and Derron, using as a boundary condition the air temperature on 1 January 2006. As that initial state is not completely real, thermal loads from 1 January 2006 to 31 December 2006 were used for computing thermal state on 1 January 2007.

560 The concrete solar absortivity was then estimated by using thermal loads from 1 January
561 2007 to 31 December 2007, with the best value being found as 0.66. Finally,
562 observations from 1 January 2008 to 31 July 2008 were employed to evaluate the model.

563 The temperatures observed and predicted at 21 concrete thermometers are depicted in
564 Fig. 8. Temperatures were predicted by the proposed model for solar radiation
565 treatment, the absence of consideration of solar radiation and the simplified sol-air
566 method for computing heat fluxes. The average model performance was assessed by the
567 statistics root mean squared error (RMSE) and bias. Results are listed in Table 3.

568 The best predictions were provided by the proposed model for solar radiation treatment.
569 Estimations by the model whose boundary conditions were computed by the sol-air
570 method are quite accurate, although RMSE increases by a 50% and 20% for years 2008
571 and 2009 and estimations are in general lower than observations. The absence of
572 consideration of solar radiation makes the model quite inaccurate. Predictions are on
573 average 3.5 ºK lower than observations and RMSE increase by a 420% and 334% for
574 years 2007 and 2008 respectively.

575 Thermometers are often situated at midpoints between dam faces. Fig. 8 shows that the
576 thinner section, the larger amplitude of observed temperature. Thermometers 1 to 10,
577 whose amplitudes are the largest, and located in the thinnest considered arch with a
578 thickness that varies from 6.35 m in the key to 8.19 m in the springing. Thermometers
579 (11) to (17) are situated in an arch with a thickness that varies from 13.63 m to 17.21 m
580 and thermometers (18) to (21) in an arch with thickness from 16.83 m to 20.73 m.
581 Observed temperature at thermometers (11) to (21) is almost constant throughout the
582 year and similar to annual mean ambient temperature.

583 Since amplitude of dam face temperature is larger than the amplitude of temperature at
584 mid-points, a thermal gradient between each point is generated. For a given section, the
585 temperature difference between mid-points and face-points is larger as the thickness of
586 the cross-section does. The largest differences are located in the lower arches where the
587 temperature at midpoints is quite constant along the year (it varies between 286.0 and
588 287.0 ºK) and slightly higher than the mean ambient temperature (285.3 ºK).
589 Accordingly, an order of magnitude of the maximum difference is the amplitude of the
590 minimum dam face temperature which from Fig. 5(b) is approximately equal to 12.0 ºK.
591 This value is slightly higher than the amplitude of the ambient temperature,
592 approximately equal to 10.5 ºK, because of solar radiation increases concrete
593 temperature.

594 The effect of solar radiation over the simulated temperatures is observed in Fig. 8. The
595 thinnest section, the largest effects of solar radiation over mean temperature. The
596 difference between predictions can be up to 6 ºK in the thinnest sections for the
597 simulations with the proposed model for solar radiation and the absence of its
598 consideration. Nevertheless, consequences of solar radiation over the amplitude of the
599 temperatures are almost negligible.

600 The performance of the model whose boundary conditions were computed by the sol-air
601 method is quite satisfactory, as it can be observed in Fig. 8. Predictions are quite similar
602 to observations. However, plotted results are from points located at midpoints between
603 dam faces. Atmospheric effects on those points are substantially dampened. For these
604 reasons, temperatures will be analyzed in other parts of the dam.

605 Fig. 9 depicts the temperature field in the central block on 4 August 2007 computed by
606 the three methodologies. The effect of solar radiation over the simulated concrete

607 temperatures is analyzed by comparing Fig. 9(a) and 9(b). The difference between
608 predictions is largest in the downstream exposed face (up to 10 ºK) and the thinnest
609 sections (up to 6 ºK).

610 Temperatures at mid-points of the sections are quite similar when solar radiation is
611 considered (Fig. 9(a) and 9(c)). However, the largest differences become when the
612 downstream exposed face of the dam and the thinnest parts are analyzed. Whereas the
613 sol-air method provides a quite uniform temperature within the range 297.7-300.3 ºK in
614 the downstream face, temperatures computed by the proposed methodology are spatially
615 more variable with magnitudes between 297.7-300.3 ºK in the upper parts of the block
616 and 302.9-305.5 ºK in the lower areas. Moreover, temperatures at the thinnest parts of
617 the dam (close to the crest) are quite different. Temperatures computed by the proposed
618 methodology are within the range 297.7-300.3 ºK and by the sol-air method 295.1-297.7
619 ºK.

620 Consequently, predictions simulated by the sol-air method are, in general, up to 5.2 ºK
621 lower than the ones calculated by the proposed methodology for solar radiation
622 treatment at the exposed faces and the thinnest parts of the dam. This phenomenon has
623 also been observed to a lesser extent when the bias of the predicted temperatures is
624 analyzed (Table 3).

625 **Structural analyses.**

626 Structural analyses have been performed at the case study. The included loads were the
627 self-weight, computed on free cantilevers, the hydrostatic and the thermal loads. The
628 reference thermal field for the zero strain was taken from the thermal field in the
629 contraction joint grouting day.

630 Fig. 10 depicts the maximum principal stress contour plots of the central block on 4
631 August 2007 which is the day with the largest radial displacements at the crest of the
632 crown cantilever. The thermal field was computed by the aforementioned thermal model
633 whose boundary conditions were assessed by the proposed method for solar radiation
634 treatment, without solar radiation and the sol-air method.

635 Stresses under thermal loads are caused by the thermal gradient between the internal
636 and external parts of the dam and the increase of the mean concrete temperature.
637 Temperatures on external dam faces are maximum in August. However, the maximum
638 temperatures on mid-face do not occur at that time. Furthermore, the magnitudes of both
639 maximum are quite different. Consequently, a thermal gradient is generated and the
640 external faces will expand more than the mid-face. The different expansions, especially
641 in the vertical direction, will cause tensile stresses in the mid-faces and compressive
642 ones in the external faces. The increase of the mean concrete temperature makes the
643 arches expand and move the crest of the cantilevers towards upstream. The
644 displacements of the crests will produce tensile stresses on an area close to the
645 downstream toe of the cantilevers, while compressive stresses on the upstream face.

646 The largest tensile stresses in the mid-face of the central block are given by the thermal
647 loads computed with the proposed method for solar radiation treatment (Fig. 10(a)).
648 This methodology provides the largest temperatures on dam faces and the crest, which
649 will generate the largest tensile stresses in the mid-face according to the previous
650 paragraph.

651 The thermal loads provided by the sol-air method generate lower tensile stresses in the
652 mid-face of the central block (Fig. 10(b)). Temperatures were lower than the ones
653 provided by the method for solar radiation treatment.

Finally, the lowest maximum principal stresses were provided by the thermal loads computed by the proposed model without solar radiation. However, larger tensile stresses are got in the lower mid-face of the dam. The absence of consideration of solar radiation and the low magnitude of the amplitude of the thermal signal may involve negative thermal loads and, consequently, the contraction of the concrete which generates tensile stresses.

An overall structural behavior of the dam is provided by the radial displacement of the crest of the crown cantilever. Moreover, this movement is often measured during the monitoring tasks. Fig. 11 plots the evolution of the movement for the year 2007 and Fig 12 the radial displacement of the central block on 4 August 2007, both due to thermal loads. Temperatures were computed by the three reported methodologies.

The largest movements are caused by the thermal loads computed with the proposed method for solar radiation treatment. The magnitude is up to 13% larger than the result provided by the thermal loads calculated with the sol-air method. The absence of consideration of solar radiation implies a reduction by up to 44%.

CONCLUSIONS.

A procedure for modeling thermal response of arch dams has been proposed. Air temperature, wind speed, solar radiation, rainfall and shading are considered when computing boundary conditions. The conditions are those of imposed heat flux in the dam faces in contact with air and of imposed temperature equal to water temperature in dam faces and abutments in contact with water. The heat diffusion equation is solved by means of the finite element method in a three-dimensional domain composed by the dam and a finite region of the foundation, with truncated areas modeled by infinite

677 boundary elements. The proposed methodology is applied to the case study, the La
678 Baells arch dam, located in the area of Barcelona.

679 Heat flux through dam faces is computed as the sum of the energy due to convection,
680 long-wave radiation exchange, evaporative cooling and solar energy. The assessment of
681 the solar energy reaching dam faces is a complex task which requires consideration of
682 the shading, curvature of dam surfaces, non-uniform orientation and slope of dam faces
683 and the change of the incident solar angle during the day due to sun movement, among
684 other variables.

685 A consistent methodology for computing boundary conditions is reported, with special
686 attention being given to solar energy. The most suitable solar models for estimating
687 hourly global solar radiation, components of solar radiation and insolation over tilted
688 surfaces are used.

689 As solar insolation over dam faces is influenced by shading, general expressions for
690 determining shaded areas in any dam and time are proposed. Moreover, in order to
691 consider the curvature of dam faces, a differential expression for computing insolation
692 over dam surfaces is proposed.

693 The reported methodology leads to accurate boundary conditions and, consequently, to
694 enhanced concrete temperature calculation. Numerical results agree well with the
695 recorded temperatures at 21 thermometers embedded in the La Baells dam. Concrete
696 temperature observations are divided into two sets for calibrating and assessing the
697 model. Whereas the first data set is estimated with a root mean square error and bias
698 equal to 0.74 ºK and -0.24 ºK respectively, the second set involves a root mean square
699 error equal to 0.98 ºK and a -0.70 ºK bias. The effect of the solar radiation over the
700 thermal field of the case study is analyzed. The absence of consideration of solar
701 radiation involves quite inaccurate predictions of temperatures, especially in the thinnest

part of the dam and the exposed faces where the magnitude can be up to 6 ºK and 10 ºK lower respectively.

The proposed methodology is compared with the simplified "sol-air temperature" method for computing heat fluxes. Temperature predictions on the exposed faces and the thinnest parts close to the crest can differ up to 5.2 ºK, providing the simplified method the lowest temperatures. However, predictions at the mid-faces are quite similar. The consequences on structural calculations are lower stresses and displacements when thermal loads are computed by the simplified method.

Thermal loads computed with the sol-air temperature method can provide accurate structural results when an overall behavior of the dam is analyzed. However, if the aim of the structural model is to analyze certain parts of the dam, i.e., the exposed faces, the reported methodology for computing thermal loads can provide more accurate results.

Since the second most major repairs in dams during operation are carried out in response to external temperature variations, thermal studies play a vital role during the design phase and during the monitoring of existing structures. The methodology can be used for computing thermal loads in other regions of the world. Furthermore, it provides a useful tool for estimating thermal stress during the service life of the dam. This may also permit easy adaptation for use in other civil infrastructure, such as bridges where thermal loads also play a vital role.

ACKNOWLEDGEMENTS.

This work was supported by the Ministerio de Economía y Competitividad (Spanish Ministry of Economy and Competitiveness) under code IPT-2012-0813-390000, titled "Desarrollo del Software iCOMPLEX para el control y evaluación de la seguridad de

725 infraestructuras críticas" (Development of the iCOMPLEX software for the control and
726 assessment of the security of critical infrastructures).

727 The authors also wish to thank the company Ofiteco and l'Agència Catalana de l'Aigua
728 (the Catalan Water Agency) for measured data from La Baells Dam.

APENDIX: Mathematical astronomy.

Solar declination is defined as the angular position of the sun at solar noon with respect to the plane of the equator. Spencer (1971) proposed the Eq.(A1) for computing the declination in radians at the day d_n of the year,

$$\delta = 0.006918 - 0.399912\cos\Gamma_d + 0.070257\sin\Gamma_d - 0.006758\cos 2\Gamma_d + 0.000907\sin 2\Gamma_d - 0.002697\cos 3\Gamma_d + 0.00148\sin 3\Gamma_d \quad \text{(A1)}$$

where Γ_d is given by Eq. (A2).

$$\Gamma_d = 2\pi\frac{d_n - 1}{365} \quad \text{(A2)}$$

The daily average extraterrestrial irradiation on a horizontal surface $H_{G,o}$ is evaluated from the solar constant I_{sc} equal to 4.921 $MJm^{-2}h^{-1}$ with:

$$\mathrm{H}_{G,o} = \frac{24}{\pi}\frac{I_{sc}}{E_o}(\cos\delta\cos\phi\sin\omega_o + \omega_o\sin\delta\sin\phi) \quad \text{(A3)}$$

where E_o is the sun-earth correction factor, ϕ is the latitude of the site in interest and ω_o is the sunrise hour angle. The hourly extraterrestrial irradiation on a horizontal surface $I_{G,o}$ for a period between the hourly angles ω_1 and ω_2 is computed by:

$$\mathrm{I}_{G,o} = \frac{24}{\pi}\frac{I_{sc}}{E_o}\left(\sin\delta\sin\phi\frac{\pi}{12} + \cos\delta\cos\phi\cos\left(\frac{\omega_2 - \omega_1}{2}\right)\sin\left(\frac{\pi}{12}\right)\right) \quad \text{(A4)}$$

Spencer (1971) recommended that E_o were estimated from Eq.(A4), where ω_o is obtained from Eq.(A5) and the day length in hours is calculated from Eq.(A6).

$$\mathrm{E}_o = 1.000110 + 0.034221\cos\Gamma_d + 0.001280\sin\Gamma_d + 0.000719\cos 2\Gamma_d + 0.000077\sin 2\Gamma_d \quad \text{(A5)}$$

$$\omega_o = -\tan\phi\tan\delta \quad \text{(A6)}$$

741 The daily-average solar elevation outside of the atmosphere α_o is computed with the
742 following expression (Gueymard 1986):

$$\sin \alpha_o = \frac{\cos \phi \cos \delta \, (\sin \omega_o - \omega_o \cos \omega_o)}{\omega_o} \tag{A7}$$

743 Solar position at the hour angle ω is defined by the angles solar altitude α and solar
744 azimuth ψ. α is the angle between the horizontal and the line to the sun and can be
745 found from Eq.(A8), where ω is calculated by Eq.(A9) as function of the local apparent
746 time t. ψ is the angular displacement from the south of the projection of sunbeams on
747 the horizontal plane and is obtained from Eq.(A10). Displacements east of south are
748 negative and west of south are positive.

$$\sin \alpha = \sin \delta \sin \phi + \cos \delta \cos \phi \cos \omega \tag{A8}$$

$$\omega = \pi(1 - t/12) \tag{A9}$$

$$\cos \psi = \frac{\sin \alpha \sin \phi - \sin \delta}{\cos \alpha \cos \phi} \tag{A10}$$

749

750

751 # NOTATION.

A	Anisotropy index
$A_{w,s}$	Annual water temperature amplitude at the surface
a	Solar absorptivity
b	Upstream face of the crown cantilever
$\mathbf{C}$	Specific heat matrix
C_s	Stefan-Boltzmann constant
c	Specific heat
c_p	Specific heat capacity of air
$\mathbf{D}$	Nodal displacement vector
d_n	Day of the year
E_o	Sun-earth correction factor
E_S	Moisture emissivity coefficient
e	Emissivity
e_{sk}	Emissivity of the sky
e_s	Saturation vapour pressure
$\mathbf{F_T}$	Vector of applied heat flows
$\mathbf{F_S}$	Vector of applied forces
g_r	Ground refrectivity
H	Depth of reservoir
H_G	Daily global insolation on a horizontal surface
$H_{G,o}$	Extraterrestrial daily global insolation on a horizontal surface
H_r	Relative humidity
h	Convection coefficient

h_t	Latent heat of evaporative water
I_G	Hourly global insolation on a horizontal surface
I_b	Hourly beam insolation on a horizontal surface
I_d	Hourly diffuse insolation on a horizontal surface
$I_{G,o}$	Extraterrestrial hourly global insolation on a horizontal surface
I_{sc}	Solar constant
$I_{n,b}$	Hourly normal beam insolation
$I_{T,G}$	Hourly global insolation on a tilted surface
$I_{T,b}$	Hourly beam insolation on a tilted surface
$I_{T,d}$	Hourly diffuse insolation on a tilted surface
$I_{T,d,iso}$	Hourly isotropic diffuse insolation on a tilted surface
$I_{T,d,cs}$	Hourly circumsolar diffuse insolation on a tilted surface
$I_{T,d,hb}$	Hourly horizon brightening diffuse insolation on a tilted surface
$I_{T,r}$	Hourly reflected insolation on a tilted surface
$\mathbf{K_T}$	Conductivity matrix
$\mathbf{K_S}$	Stiffness matrix
K_t	Daily global clearness index
k_t	Hourly global clearness index
k_d	Hourly diffuse fraction
n_i	Quadratic function
P	Total air pressure
q	Heat flux
q_c	Heat flux due to convection
q_{ev}	Heat flux due to water evaporation

q_m Moisture evaporative flux

q_r Heat flux due to electromagnetic radiation exchange between the dam and the surrounding air

q_s Heat flux due to solar radiation

r_o Ratio of extraterrestrial hourly global insolation to daily global insolation

r_d Radii of curvature of the downstream horizontal arch curves

r_u Radii of curvature of the upstream horizontal arch curves

r_t Ratio of hourly global insolation to daily global insolation

s Slope of the crown cantilever at the crest

t Time

t_c Thickness of the crown cantilever

t_o Day at which ambient temperature is maximum

α Solar altitude angle

α_o Extraterrestrial daily-average solar elevation angle

β Slope of surface

δ Solar declination angle

$\boldsymbol{\theta}_{\mathrm{n}}$ Vector of nodal temperatures at time $\mathrm{t_n}$

θ Concrete temperature

θ_a Air temperature

θ_{dp} Dew point temperature

θ_e Sol-air temperature

θ_w Water temperature

$\overline{\theta_{w,b}}$ Mean annual water temperature at the bottom of the reservoir

$\overline{\theta_{w,s}}$	Mean annual water temperature at the surface of the reservoir
ϑ	Transient integration parameter
λ	Thermal conductivity
ρ	Density
ϕ	Latitude
ψ	Solar azimuth angle
ω	Solar hour angle
ω_o	Sunrise hour angle
ω_w	Angular frequency of the water temperature
Γ	Dam faces domain
$\Gamma_{d,k}$	k^{th} dam face sub-domain from the downstream face
$\Gamma_{u,k}$	k^{th} dam face sub-domain from the upstream face
$\Gamma_{s,k}$	Part of the k^{th} dam face sub-domain exposed to sunbeams

752

753

754 # REFERENCES.

755 Agullo, L., Mirambell, E., and Aguado, A. (1996). "A model for the analysis of concrete
756 dams due to environmental thermal effects". International Journal of Numerical
757 Methods for Heat & Fluid Flow, 6(4), 25-36.

758 ASHRAE (2001). ASHRAE Handbook: fundamentals. American Society of Heating,
759 Refrigerating and Air Conditioning Engineers, Atlanta, GA, USA.

760 Azenha, M. and Faria, R. (2008). "Temperatures and stresses due to cement hydration
761 on the R/C foundation of a wind tower- A case study." Engineering structures, 30(9),
762 2392-2400.

763 Azenha, M. (2009). "Numerical simulation of the structural behaviour of concrete since
764 its early ages". PhD thesis, Faculty of Engineering of the University of Porto, Porto,
765 Portugal.

766 Badescu, V. (2002). "3D isotropic approximation for solar diffuse irradiance on tilted
767 surfaces." Renewable Energy, 26(2), 221-233.

768 Batlles, F.J, Rubio, M.A., Tovar, J., Olmo, F.J. and Alados-Arboledas, L. (2000).
769 "Empirical modeling of hourly direct irradiance by means of hourly global irradiance."
770 Energy, 25(7), 675-688.

771 Bentz, D.P. (2000). A computer model to predict the surface temperature and time-of-
772 wetness of concrete pavements and bridge decks. US Department of Commerce,
773 NISTIR 6551, available at http://ciks.cbt.nist.gov/bentz/nistir6551/tpredict.html.

774 Bentz, D.P. and Turpin, R. (2007). "Potential applications of phase change materials in
775 concrete technology." Cement & Concrete Composites, 29, 527-532.

776 Bofang, Z. (1997). "Prediction water temperature in deep reservoirs." Dam Engineering,
777 8(1), 13-25.

778 Boutillon, L., Linger, L., Kolani, B. and Meyer, E. (2012). "Effects of sun irradiation on
779 the temperature and early age stress distribution in outdoor concrete structures." In
780 RILEM-JCI International Workshop on Crack Control of Mass Concrete and Related
781 Issues Concerning Early-Age of Concrete Structures, Paris, France.

782 Briffaut, M., Benboudjema, F., Torrenti, J.M. and Nahas, G. (2011). "A thermal active
783 restrained shrinkage ting test to study the early age concrete behaviour of massive
784 structures". Cement and Concrete Research, 41(1), 56-63.

785 Briffaut, M., Benboudjema, F., Torrenti, J.M. and Nahas, G. (2012). "Effects of early-
786 age thermal behaviour on damage risks in massive concrete structures." European
787 Journal of Environmental and Civil Engineering, 16:5, 589-605.

788 Chen, B., Clark, D., Maloney, J., Mei, W. and Kasher, J. (1995). "Measurement of night
789 sky emissivity in determining radiant cooling from cool storage roofs and roof ponds."
790 In Proceedings of the National Passive Solar Conference, Vol. 20, pp. 310-313.
791 American Solar Energy Society Inc.

792 Chuntranuluck, S., Wells, C.M. and Cleland, A.C. (1998). "Prediction of chilling times
793 of foods in situations where evaporative cooling is significant-Part 1. Method
794 development." Journal of food engineering, 37(2), 111-125.

795 Collares-Pereira, M. and Rabl, A. (1979). "The average distribution of solar radiation-
796 correlations between diffuse and hemispherical and between daily and hourly insolation
797 values." Solar Energy, 22(2), 155-164.

798 Daoud, M., Galanis, N. and Ballivy, G. (1997). "Calculation of the periodic temperature
799 field in a concrete dam." Canadian Journal of Civil Engineering, 24(5), 772-784.

800 De Miguel, A., Bilbao, J., Aguiar, R. Kambezidis, H. and Negro, E. (2001). "Diffuse
801 solar irradiation model evaluation in the north Mediterranean belt area." Solar Energy,
802 70(2), 143-53.

803 Diez-Mediavilla, M., De Miguel, A. and. Bilbao, J. (2005). "Measurement and
804 comparison of diffuse solar irradiance models on inclined surfaces in Valladolid
805 (Spain)." Energy Conversion and Management, 46(13), 2075-2092.

806 Douglas, K.J. (2002). "The shear strength of rock masses." Ph. D. thesis, The University
807 of New South Wales, Sydney, NSW, Australia.

808 Duffie, J.A. and Beckman, W.A. (2013). Solar engineering of thermal processes, 4th
809 ed., John Wiley & Sons, Inc, Hoboken, NJ, USA.

810 El-Sebaii, A., Al-Hazmi, F.S., Al-Ghamdi A.A. and Yaghmou, S.J. (2010). "Global,
811 direct and diffuse solar radiation on horizontal and tilted surfaces in Jeddah, Saudi
812 Arabia." Applied Energy, 87(2), 568-576.

813 Faria, R., Azenha, M. and Figueiras, J.A. (2006). "Modelling of concrete at early ages:
814 application to an externally restrained slab." Cement & Concrete Composites, 28, 572-
815 585.

816 Gueymard, C. (2000). "Prediction and performance assessment of mean hourly global
817 radiation." Solar Energy, 68(3), 285-303.

818 Gueymard, C. (1986). "Monthly averages of the daily effective optical air mass and
819 solar related angles for horizontal or inclined surfaces." Journal of Solar Energy
820 Engineering, 108(4), 320-324.

821 Hughes, T.J R. (2000). The finite element method. Linear static and dynamic finite
822 element analysis, Dover Publications, USA.

823 Incropera, F.P., Lavine, A.S. and. De Witt, D.P. (2011). Fundamentals of heat and mass
824 transfer, 7th ed., John Wiley & Sons Incorporated, USA.

825 Jamil Ahmad, M. and Tiwari, G.N. (2008). "Study of models for predicting the mean
826 hourly global radiation from daily summations." Open Environmental Sciences, 2, 6-14.

827 Jin, F., Chen, Z., Wang, J. and Yang, J. (2010). "Practical procedure for predicting non-
828 uniform temperature on the exposed face of arch dams." Applied Thermal Engineering,
829 30(14), 2146-2156.

830 Lawrence, M.G. (2005). "The relationship between relative humidity and the dewpoint
831 temperature in moist air: A simple conversion and applications." Bulletin of the
832 American Meteorological Society, 86(2), 225-233.

833 Levinson, R. and Akbari, H. (2002). "Effects of composition and exposure on the solar
834 reflectance of portland cement concrete." Cement and Concrete Research, 32(11), 1679-
835 1698.

836 Léger, P., Venturelli, J. and Bhattacharjee, S.S. (1993a). "Seasonal temperature and
837 stress distributions in concrete gravity dams. part I: Modelling." Canadian Journal of
838 Civil Engineering, 20(6), 999-1017.

839 Léger, P., Venturelli, J. and Bhattacharjee, S.S. (1993b). "Seasonal temperature and
840 stress distributions in concrete gravity dams. part 2: Behaviour." Canadian Journal of
841 Civil Engineering, 20(6), 1018-1029.

842 Léger, P. and Leclerc, M. (2007). "Hydrostatic, temperature, time-displacement model
843 for concrete dams." Journal of Engineering Mechanics, 133(3), 267-277.

844 Liu, C. and DeWolf, J.T. (2007). "Effect of temperature on modal variability of a
845 curved concrete bridge under ambient loads." Journal of Structural Engineering, 133,
846 1742-1751.

847 Liu, B.Y.H. and Jordan, R.C. (1963). "A rational procedure for predicting the long term
848 average performance of flat plate solar energy collectors." Solar Energy, 7(2), 53:74.

849 Liu, B.Y.H. and Jordan, R.C. (1960). "The interrelationship and characteristic
850 distribution of direct, diffuse and total solar radiation." Solar Energy, 4(3), 1-19.

851 Myers, T., Fowkes, N. & Ballim, Y. (2009). "Modeling the cooling of concrete by piped
852 water." Journal of Engineering Mechanics, 135(12), 1375-1383.

853 Mirambell, E. and Aguado, A. (1990). "Temperature and stress distributions in concrete
854 box girder bridges." Journal of Structural Engineering, 116(9), 2388-2409.

855 Muneer, T. (2004). Solar radiation and daylight models. 2nd ed, Elsevier, Oxford, UK.

856 Noorian, A.M., Moradi, I. and Kamali, G.A. (2008). "Evaluation of 12 models to
857 estimate hourly diffuse irradiation on inclined surfaces." Renewable Energy, 33(6),
858 1406-1412.

859 Palyvos, J.A. (2008). "A survey of wind convection coefficient correlations for building
860 envelope energy systems' modeling." Applied Thermal Engineering, 28(6), 801-808.

861 Perez, R., Seals, R., Ineichen, P., Stewart, R. and Menicucci, D. (1987). "A new
862 simplified version of the perez diffuse irradiance model for tilted surfaces." Solar
863 Energy, 39(3), 221-231.

864 Reindl, D.T., Beckman, W.A. and Duffie, J.A. (1990). "Diffuse fraction correlations."
865 Solar Energy, 45(1), 1-7.

866 Reindl, D.T, Beckman, W.A. and Duffie, J.A. (1990). "Evaluation of hourly tilted
867 surface radiation models." Solar Energy, 45(1), 9-17.

868 Roberts-Wollman, C.L., Breen, J.E. and Cawrse, J. (2002). "Measurements of thermal
869 gradients and their effects on segmental concrete bridge." Journal of Bridge
870 Engineering, 7, 166-174.

871 Sakulich, A.R. and Bentz, D.P. (2012a). "Incorporation of phase change materials in
872 cementitious systems via fine lightweight aggregate." Construction and Building
873 Materials, 35, 483-490.

874 Sakulich, A.R. and Bentz, D.P. (2012b). "Increasing the service life of bridge decks by
875 incorporating phase-change materials to reduce freeze-thaw cycles." Journal of
876 Materials in Civil Engineering, 24, 1034-1042.

877 Sheibany, F. and Ghaemian, M. (2006). "Effects of environmental action on thermal
878 stress analysis of Karaj concrete arch dam." Journal of Engineering Mechanics, 132(5),
879 532-544.

880 Soler, A. and Gopinathan, K.K. (1994). "Estimation of monthly mean hourly global
881 radiation for latitudes in the 1 N-81 N range." Solar Energy, 52(3), 233-239

882 Spencer, JW. (1971). "Fourier series representation of the position of the sun." Search,
883 2(5).

884 Stucky, A. and Derron, M.H. (1957). Problèmes thermiques posés par la construction
885 des barrages-rèservoirs, P. Feissly, ed., Science & Technique, Lausanne, Switzerland.

886 Tham, Y., Muneer, T. and Davison, B. (2010). "Estimation of hourly averaged solar
887 irradiation: evaluation of models." Building Services Engineering Research and
888 Technology, 31(1), 9-25.

889 Ulm, F. and Coussy, O. (2001). "What is a "massive" concrete structure at early ages?
890 Some dimensional arguments." Journal of Engineering Mechanics, 127(5), 512-522.

891 US Deparment of the Interior (1977). Design of Arch Dams, 1st ed. Bureau of
892 Reclamation, Denver, CO, USA, pp. 258.

893 Wojcik, G.S., Fitzjarrald, D.R. and Plawsky, J.L. (2003). "Modelling the interaction
894 between the atmosphere and curing concrete bridge decks with the SLABS model."
895 Meteorological Applications, 10(2), 165-186.

896 Yu, Z.Z. and Wang, L.L. (2011). "Factors influencing thermal structure in a tributary
897 bay of Three Gorges Reservoir". Journal of Hydrodynamics, Ser. B, 23(4), 407-415.

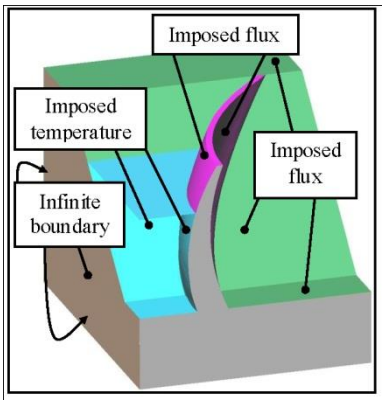

Figure 1: Boundary conditions.

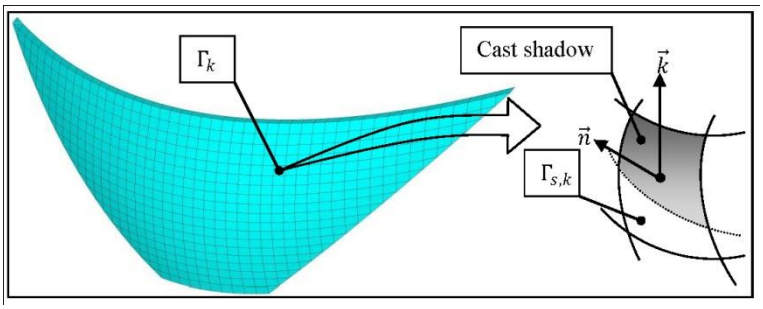

Figure 2: Spatial discretizacion of dam faces.

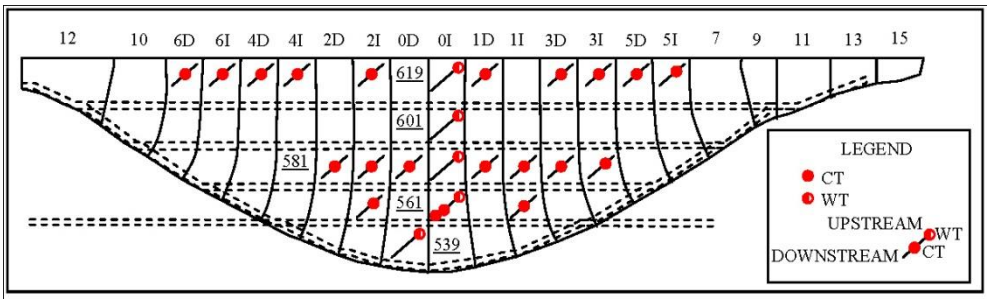

902
903 Figure 3: The La Baells dam. Thermometers.

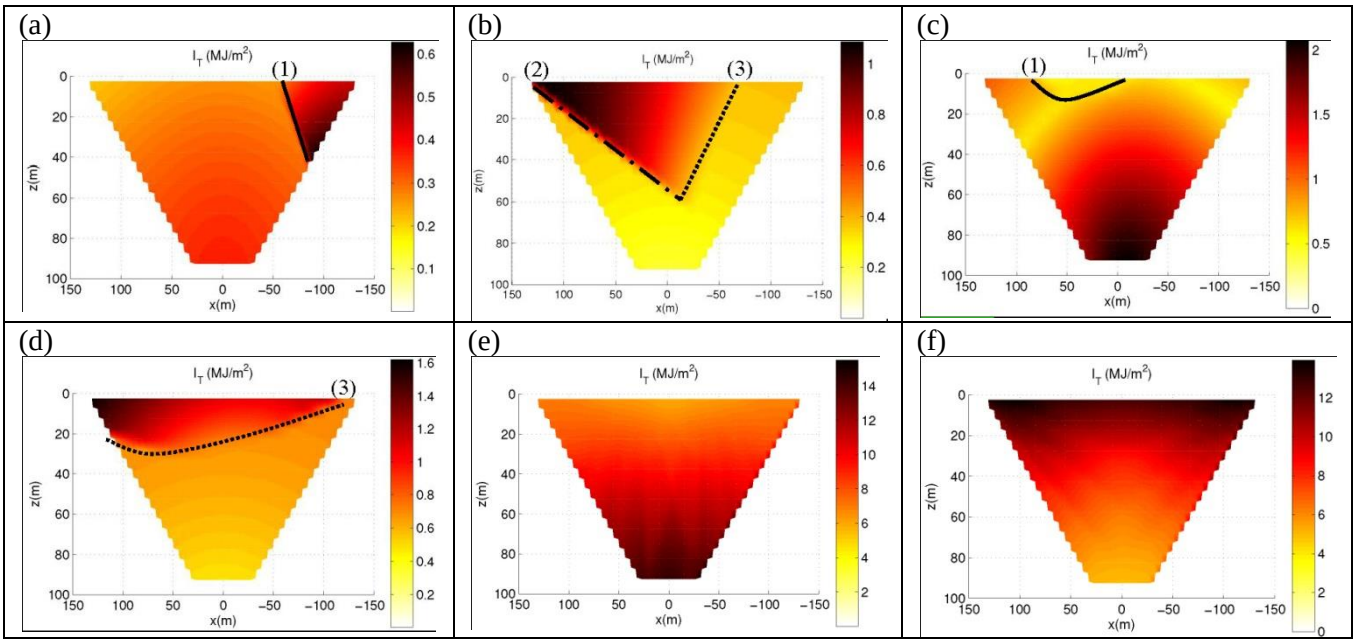

Figure 4: Hourly insolation on 5 July 2007 on (a) downstream face over 6:00 to 7:00 period, (b) upstream face over 6:00 to 7:00, (c) downstream face over 11:00 to 12:00, (d) upstream face over 11:00 to 12:00 (e) downstream over the complete day and (f) upstream over the complete day. Shading at midpoint of the hourly interval, (1) projection of the downstream edge of the crown cantilever, (2) projection of the edge of the abutment, (3) points tangent to sunrays. Hours in local apparent time.

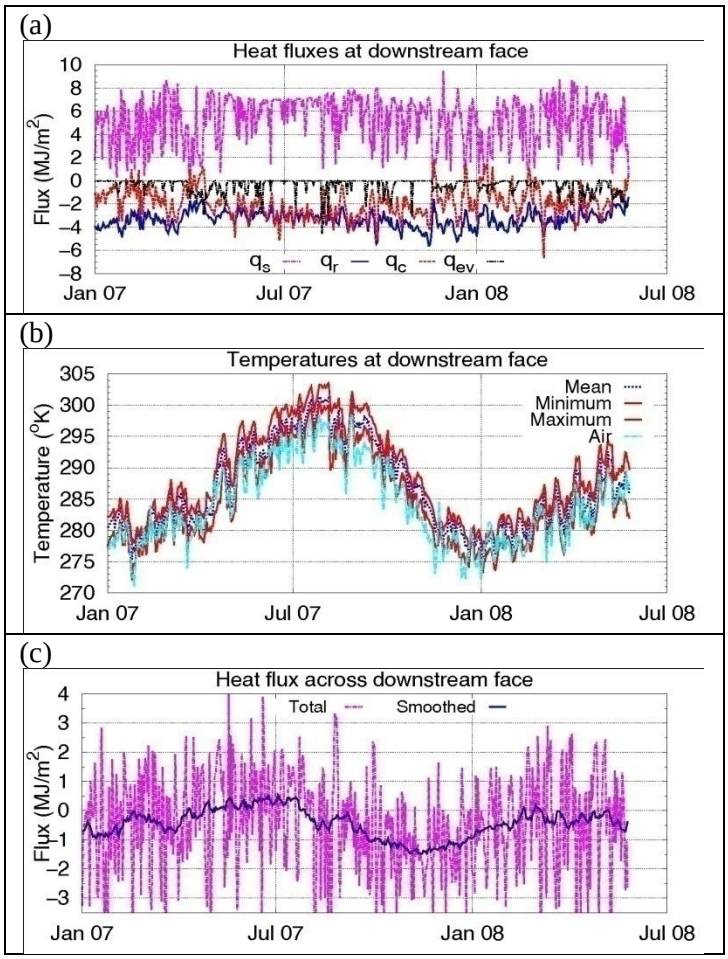

910

911 Figure 5: (a) Heat fluxes at downstream face, (b) temperatures at downstream face and (c)
912 smoothed total heat flux at downstream face.

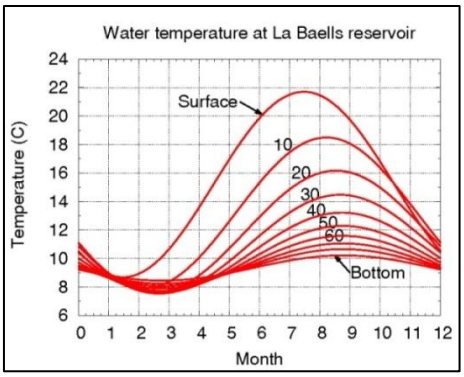

913

914 Figure 6: Water temperature at the La Baells reservoir for several depths estimated by Bofang
915 model.

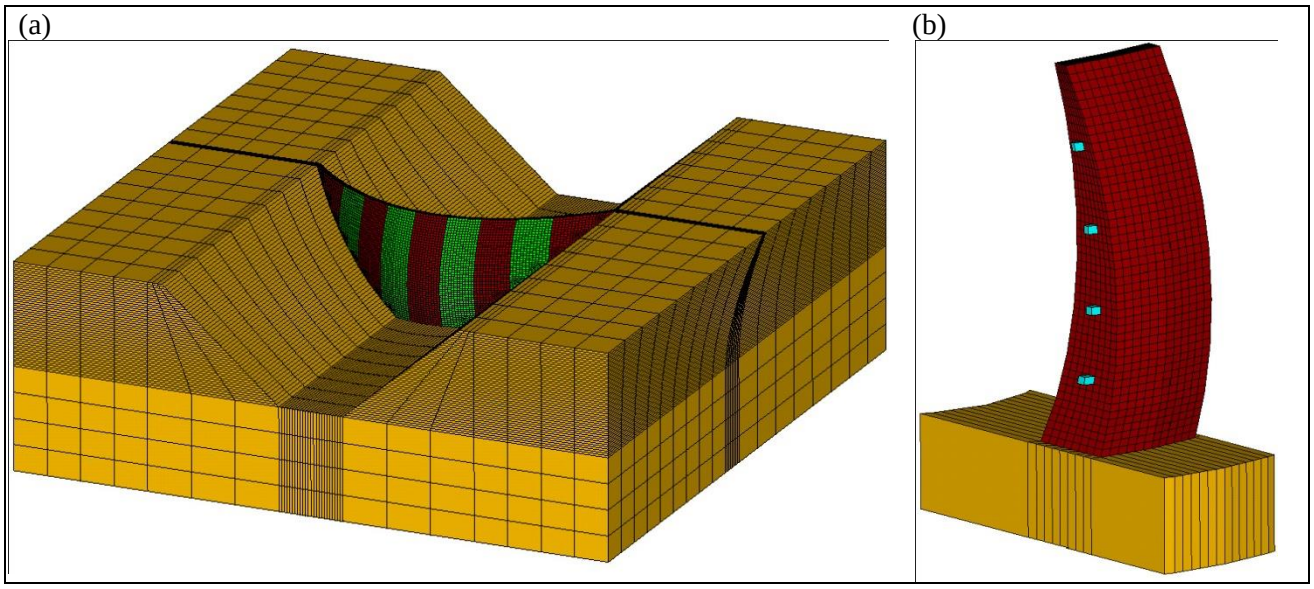

916 Figure 7: Adopted finite element mesh.

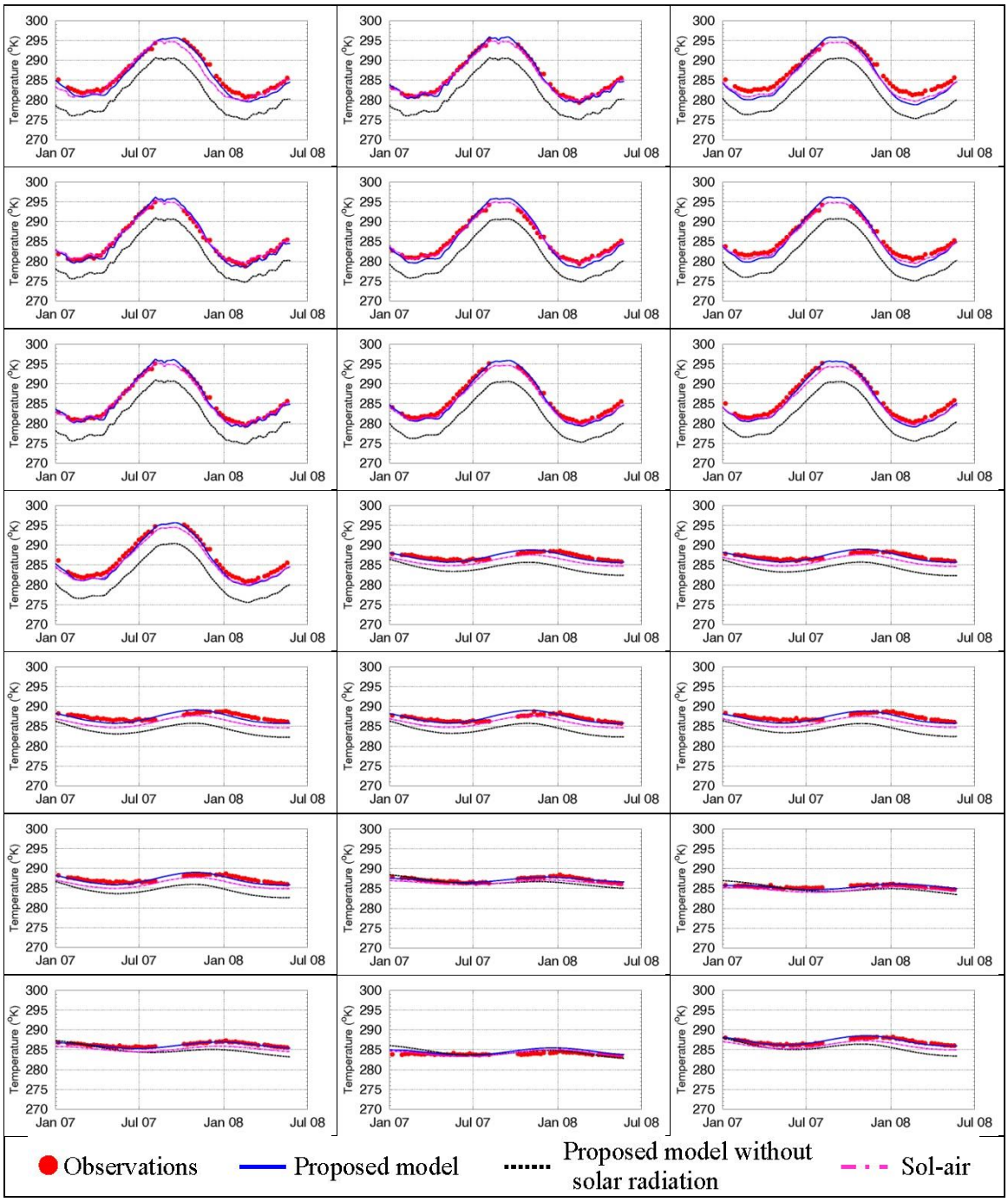

Figure 8: Observed and predicted temperature at several concrete thermometers. From top to bottom and left to right (1) CT-619-6D, (2) CT-619-6I, (3) CT-619-4D, (4) CT-619-4I, (5) CT-619-2I, (6) CT-619-1D, (7) CT-619-3D, (8) CT-6193I, (9) CT-619-5D, (10) CT-619-5I, (11) CT-581-2D, (12) CT-581-2I, (13) CT-581-0d, (14) CT-581-1D, (15) CT-581-1I, (16) CT-581-3D, (17) CT-581-3I, (18) CT-561-2I, (19) CT-561-0I2, (20) CT-561-0I3 and (21) CT-561-1I.

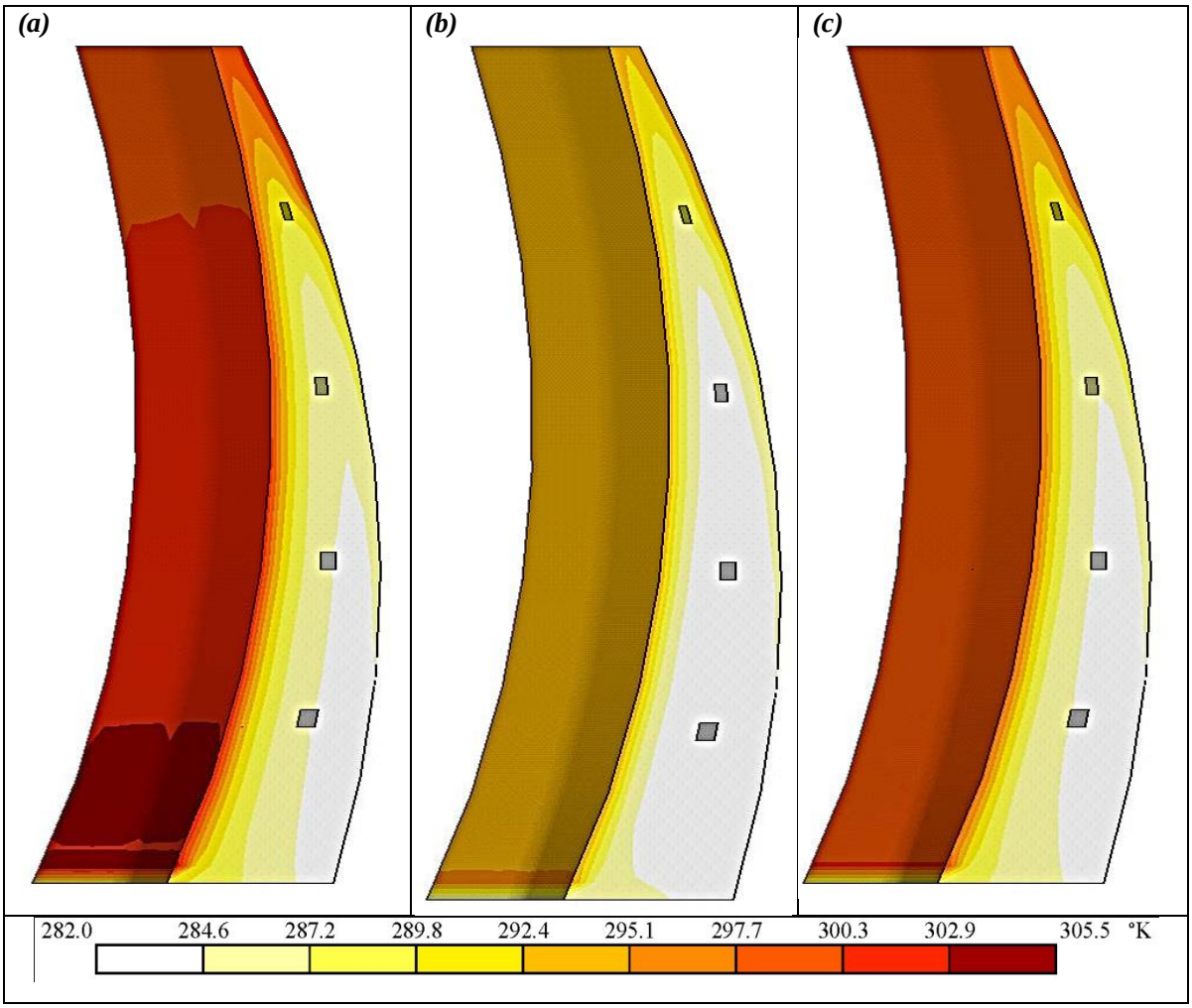

Figure 9: Temperatures of the central block on 4 August 2007. Thermal boundary conditions are computed by (a) proposed method for solar radiation treatment, (b) proposed method without solar radiation and (c) sol-air method.

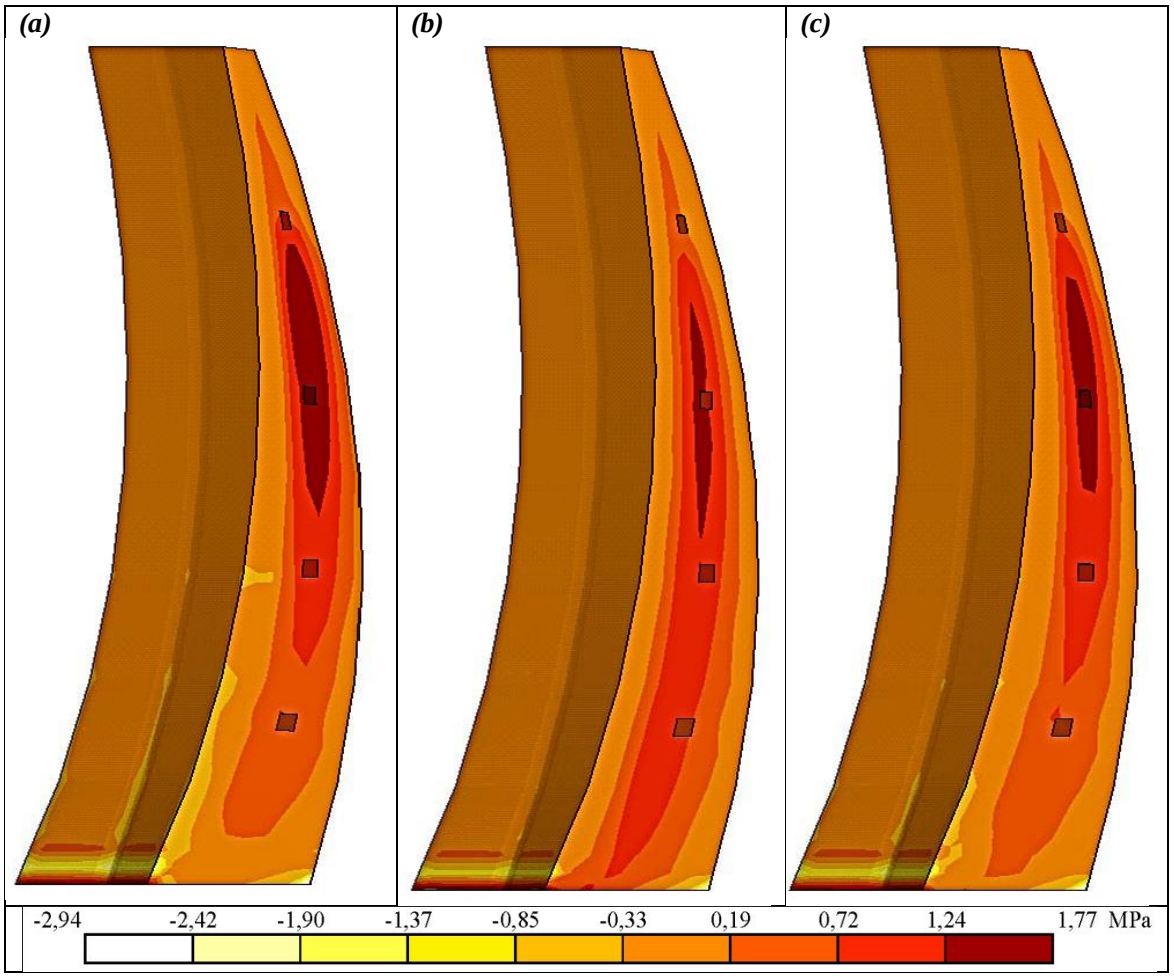

928
929 Figure 10: Maximum principal stress contour plots of the central block on 4 August 2007
930 including self-weight, thermal and hydrostatic loads. Thermal boundary conditions are
931 computed by (a) proposed method for solar radiation treatment, (b) proposed method without
932 solar radiation and (c) sol-air method. Tensile stresses are positive.
933

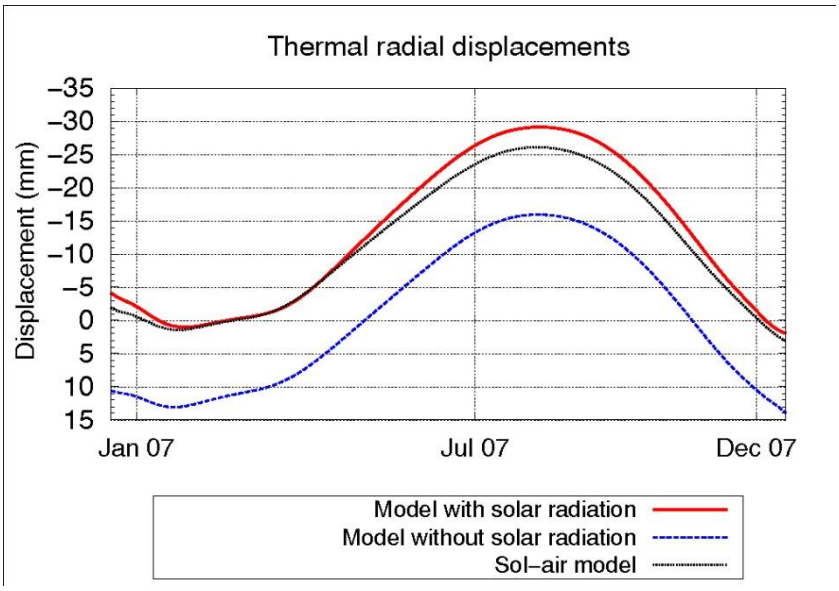

934

935 Figure 11: Evolution of the thermal radial displacements at the crest of the crown cantilever.
936 Positive displacements are towards downstream.
937

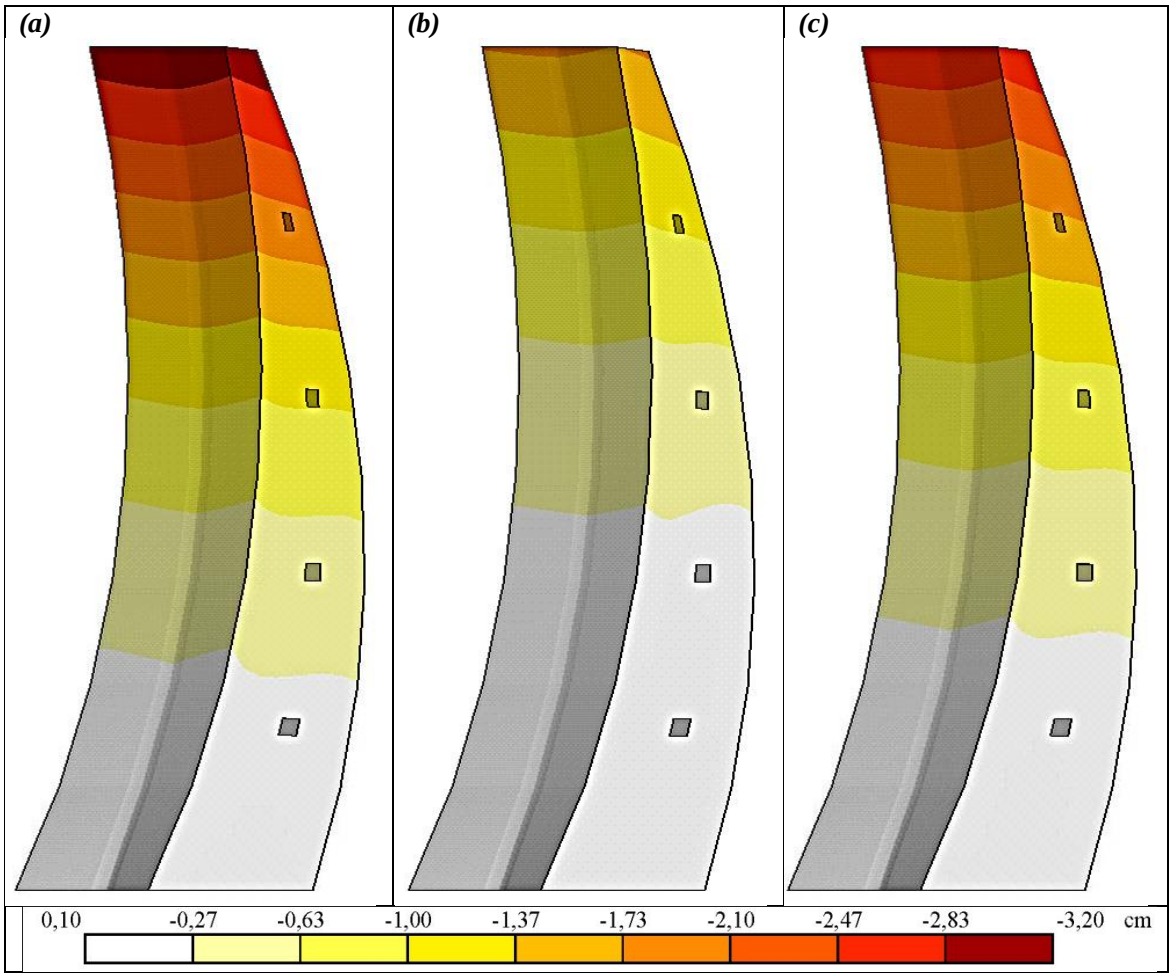

Figure 12: Thermal radial displacements of the central block on 4 August 2007. Thermal boundary conditions are computed by (a) proposed method for solar radiation treatment, (b) proposed method without solar radiation and (c) sol-air method. Positive displacements are towards downstream.

Thermometer	T.(m)	D.D.(m)	Thermometer	T.(m)	D.D.(m)	Thermometer	T.(m)	D.D.(m)
CT-619-6D	8.16	4.89	CT -619-3I	7.21	4.39	CT -581-1I	15.21	9.51
CT -619-6I	7.77	4.58	CT -619-5D	7.77	4.58	CT -581-3D	17.16	10.50
CT -619-4D	7.21	4.39	CT -619-5I	8.19	5.92	CT -581-3I	17.21	6.20
CT -619-4I	6.92	4.12	CT -581-2D	15.2	9.51	CT -561-2I	18.10	13.23
CT -619-2I	6.35	3.68	CT -581-2I	14.20	8.73	CT -561-0I-2	16.83	10.08
CT -619-1D	6.35	3.68	CT -581-0D	13.63	6.57	CT -561-0I-3	16.83	5.85
CT -619-3D	6.92	4.12	CT -581-1D	14.20	6.95	CT -561-1I	20.73	9.98

944 Table 1: Position of thermometers. T.=thickness at thermometer position. U.D.= distance from
945 downstream face to thermometer. CT-619-6D= concrete thermometer situated at the 619 m
946 above the sea level in the block 6D.

947

Material	Foundation	Concrete
Density (kg m^{-3})	3000	2400
Thermal conductivity ($WK^{-1}m^{-1}$)	2.20	2.43
Specific heat ($JKg^{-1}K^{-1}$)	950	982
Emissivity	0.70	0.70

948 Table 2: Properties of the foundation and the concrete

949

Year	2007		2008	
	RMSE	**BIAS**	**RMSE**	**BIAS**
Proposed model for solar radiation	0.74	-0.24	0.98	-0.70
Proposed model without solar radiation	3.85	-3.30	4.25	-3.94
Sol-air method	1.05	-0.83	1.18	-0.95

950 Table 3: Performance of the thermal models in ºK.
951